ANALYSIS OF PARTICULATE MATTER (PM) AND LUNG DEPOSITED SURFACE AREA (LDSA) CONCENTRATIONS IN OPERATIONAL AREAS OF A ROOM-AND-PILLAR OIL SHALE MINE

by

RUSLANA KORSHUNOVA

THESIS SUPERVISOR

SERGEI SABANOV

THESIS

Thesis submitted to the School of Mining and Geosciences of Nazarbayev University in Partial Fulfillment of the Requirements for the Degree of **Master of Science in Mining Engineering**

Nazarbayev University

April 10, 2025

ORIGINALITY STATEMENT

I, Ruslana Korshunova, hereby declare that this submission is my own work and to the best of my knowledge it contains no materials previously published or written by another person, or substantial proportions of material which have been accepted for the award of any other degree or diploma at Nazarbayev University or any other educational institution, except where due acknowledgement is made in the thesis.

Any contribution made to the research by others, with whom I have worked at NU or elsewhere is explicitly acknowledged in the thesis.

I also declare that the intellectual content of this thesis is the product of my own work, except to the extent that assistance from others in the project's design and conception or in style, presentation and linguistic expression is acknowledged.

Signed on April 10, 2025

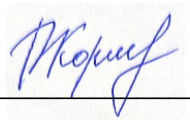

ABSTRACT

Particulate matter (PM) in the context of underground mining results from various operations such as rock drilling and blasting, ore loading, hauling, crushing, dumping, and from diesel exhaust gases as well. These operations result in the formation of fine particles that can accumulate in the lungs of mineworkers. The lung deposited surface area (LDSA) concentration is a variant solution to evaluate potential health impacts. The aim of this study is to analyse PM and LDSA concentrations in operational areas of a room-and-pillar oil shale mine. Measurements were carried out by a direct-reading real-time PM monitor, Dusttrak DRX, and a multimetric fine particle detector, Naneous Partector 2, during the loading and dumping processes using the diesel engine loader. Consequently, the analysis was conducted on PM, LDSA, particle surface area concentration (SA), average particle diameter (d), particle number concentration (PNC), and particle mass ($PM_{0.3}$), producing a few valuable correlation factors. Averaged LDSA was around 1433 $\mu m^2/cm^3$ and reached maximum peaks of 2140 $\mu m^2/cm^3$ during the loading, which was mostly related to diesel exhaust emissions, and within the dumping, 730 $\mu m^2/cm^3$ and 1840 $\mu m^2/cm^3$, respectively. At the same time, average PM_1 was about 300 $\mu g/ m^3$ during the loading, but within the dumping peaks, it reached up to 10,900 $\mu g/m^3$. During the loading phase, particle diameter ranged from 30 to 90 nm, while during the dumping phase peaks, it varied from 90 to 160 nm. On this basis, a relationship between PNC and particle diameter has been produced to demonstrate an approximate split between diesel particulate matter (DPM) and oil shale dust diameters. The Ventsim simulation demonstrated a potential concentration of diesel and dust particles in a remote area of the mine where no direct measurements had been conducted. This study offers important data on PM and LDSA concentration that can be used for estimating potential exposure to miners at various working operations in the room and pillar oil shale mine, and will be used for air quality control in accordance with establishing toxic aerosol health effects.

ACKNOWLEDGMENT

I am deeply grateful to all those who have supported and guided me throughout the journey of completing my master's thesis.

First and foremost, I extend my sincere appreciation to my advisor, Sergei Sabanov, for his invaluable guidance, insightful feedback, and continuous encouragement. His expertise and dedication were crucial in shaping my research and keeping me motivated through every challenge.

I am also thankful to the faculty members of Nazarbayev University who shared their knowledge and offered meaningful suggestions that enriched my work.

I would like to acknowledge the financial support provided by the Nazarbayev University Grant Program (Research Grant #0122022FD4128), which made this research possible.

Finally, I am deeply thankful to my family and friends for their unwavering belief in me. Their patience, understanding, and love gave me the strength to persevere.

Thank you all for being part of this remarkable journey.

TABLE OF CONTENTS

LIST OF FIGURES

LIST OF TABLES

1. INTRODUCTION

1.1 Problem Definition

The mining industry, especially in the field of underground oil shale and coal mining, plays a role in the global energy economy. Thus, major coal-rich countries, such as India and China, together with leading oil shale countries, such as China and Brazil, play a key role in the global energy sector, making a significant contribution to global coal consumption and oil shale production (World Energy Outlook, 2022). However, in addition to the different economic benefits, this activity has a number of negative aspects related to the impact on the health of humanity, particularly in terms of respiratory and pulmonary diseases (Chang & Xu, 2017). There is an increasing amount of literature that recognizes the importance of accurate monitoring of air particles in the working environment and their impact on the health of miners, especially in the context of two main aspects: the measurement of particle matters in the air (Particle Matters - PMs) and the assessment of the deposition area of particles in the lungs (Lung Deposition Surface Area - LDSA) (Wang et al., 2019b). According to Du et al. (2022), particle matters in the context of the mining industry are the smallest solid particles resulting from various mining operations, namely rock drilling, blasting, loading, transportation inside mines and exhaust of mine vehicles. These actions lead to the formation of dust particles, which, as a result, can deposit in the lungs of mine workers (Patra et al., 2016a). In order to determine the potential impact of these solid particles on health, researchers use the LDSA indicator (Lepistö et al., 2023). The authors define LDSA as the surface area of particles that settle in the alveoli of the human respiratory system. Moreover, the authors claim that the type of particles, in particular composition and size, play a significant role in determining this indicator. LDSA has been shown to be strongly associated with adverse health effects, as it more accurately reflects the dose of inhaled nanoparticles that interact with lung tissue, contributing to respiratory and cardiovascular diseases. However, the main problem is the fact that none of the previous studies investigated the measurements and monitoring of PMs in relation to LDSA concentrations in underground mines, moreover, there remains limited understanding about the unique characteristics of particulates produced specifically in oil shale operational environments. This indicates a need to research the various perceptions of methods of measurement and monitoring of PMs and LDSA specific to underground oil shale mines.

1.2 Objectives of the Thesis

1.2.1 Main Objectives

The main objective of the study is to analyze the PM and LDSA concentration in the operational faces of an oil shale underground mine environment. This includes analysis of PMs, LDSA, particle surface area concentration (SA), average particle diameter (d), particle number concentration (PNC), and particle mass ($PM_{0.3}$), as well as assessing their potential health implications for workers.

1.2.2 Specific Objectives

To achieve the primary objective of the study, the subsequent sub-objectives must be fulfilled:

- To analyze the concentration of various PM fractions (PM_1, $PM_{2.5}$, PM_{10}) in different zones of the mine using received experimental measurements data;
- To build a mine ventilation model to validate experimental data;
- To estimate the relationship between different air quality metrics indicators, namely PMs, LDSA, SA, PNC and average particle diameter;
- To determine the morphology of particulate matter and its correlation with elemental composition and toxicity;
- To produce Monte Carlo modelling to demonstrate the range of outcomes;
- To suggest future approaches for determining exposure limits and health standards for miners.

1.3 Hypotheses

Based on theoretical assumptions, the following hypotheses were formulated in the study:

- In the underground mining environment, the concentration of particulate matter (PM) and the lung deposition surface area (LDSA) have a particular relationship, suggesting that higher PM levels are linked to a higher risk of respiratory deposition;
- The concentration of PM can have wide variation in different areas of operation of the mine, and these fluctuations may be affected by specific types of mining and environmental conditions, which lead to different risks of exposure to workers.

1.4 Justification of the R&D

The research conducted as part of this work is justified by the urgent need to understand and reduce the potential health hazards associated with nanoparticle exposure in underground oil shale mining environments. Through careful analysis of PMs, including their size distribution and elemental composition, this study attempts to fill a significant gap in knowledge about the behavior and effects of ultrafine particles on the human respiratory system. The special attention to LDSA again highlights the importance of understanding that these particles can reach deep layers of the lungs and deposit in them, where they can pose significant health risks. It is expected that the results of this study will serve as a basis for the development of more effective impact assessment strategies and air quality control.

1.5 Scope of Work

This study will focus on the following major areas:

- **Data collection**: Collecting data from experimental measurements of PMs and LDSA in various operational zones of an oil shale underground mine;
- **Data Analysis**: Analyzing the relationship between PM concentrations, LDSA and different air quality metrics indicators using stochastic modelling.
- **Software Simulation:** Quantitative estimation of particle distribution, highlighting areas of high concentration and possible accumulation.
- **Morphological Characterization**: Characterizing the morphology and composition of particulate samples through scanning electron microscopy (SEM) and energy dispersive X-ray spectroscopy (EDS).
- **Recommendations**: Providing recommendations for further studies and real-world implementations of occupational health and safety regulations.

2. LITERATURE REVIEW

2.1 Air Quality in Underground Mines

The origins of particle emissions in underground mines are mining activities, diesel engine vehicles, and blasting operations (McDonald et al., 2003; Ghose, 2007; Saarikoski et al., 2018; Timonen et al., 2018). Dust concentrations depend on mining activities (McDonald et al., 2002) and can contain crystalline silica that can cause silicosis, lung cancer, and other diseases of the respiratory system (Straif et al., 2009; Leung et al., 2012). The issue of air quality has consistently been a matter of great concern because the dust generated during mining seriously affects the quality of underground air and worker health (Li et al., 2023; Liu & Zhou, 2015). The authors state that most of the studies prefer to neglect the assessment of air quality in underground mines, confining themselves to the analysis and forecasting. However, the unique conditions of underground mines, with their increased concentration of gases and solid particles, make it urgent to apply the air quality index (AQI) for effective monitoring and maintenance of safe working conditions.

According to Harrison (1984), AQI encompasses the assessment of five exhaust pollutants, namely carbon monoxide (CO), nitrogen oxide (NO), nitrogen dioxide (NO_2) sulfur dioxide (SO_2), and respirable combustible dust (RCD) or particulate matter (PM_{10} and $PM_{2.5}$), based on a time-weighted-average approach. The Bureau of Mines (1987) proposed that the values of pollutants and particle matters measured underground, as well as the threshold limit values (TLV) for each of them, are used to calculate the numerical value of AQI using the formulas below:

$$AQI(gas) = \frac{CO}{TLV\ for\ CO} + \frac{NO}{TLV\ for\ NO} + \frac{NO_2}{TLV\ for\ NO_2} \quad (1)$$

$$AQI(particulate) = \frac{RCD}{TLV\ for\ RCD} + \frac{SO_2}{TLV\ for\ SO_2} + \frac{RCD}{TLV\ for\ RCD} + \frac{NO_2}{TVL\ for\ NO_2} + \frac{RCD}{TLV\ for\ RCD} \quad (2)$$

According to French and other experts (Bureau of Mines, 1987), an AQI value of 3.0 to 4.0 constitutes a moderate concern to health, which could be mitigated by personal protective measures such as respirators or filters, while a number more than 4.0 indicates a degree of health hazard and the requirement for improved ventilation or pollutant source controls to reduce the value to less than 3.0.

Thus, the primary objective of evaluating underground air quality is to ensure that the levels of detrimental gases and particulate matter are not above the established maximum allowable

thresholds (Li et al., 2023). A number of researchers use different models for the evaluation of air quality, for example, Liu et al. (2015) used the matter-element model for the evaluation of air quality in metal mines. The study involved the determination of the classic domain matrix, node domain matrix, and weights, which were subsequently used to create the assessment levels. This novel approach contributes to the field of underground air quality evaluation. On the other hand, Shi et al. (2006) evaluated the air quality in metal mines using the pollution loss rate method and the idea that the concentration of pollutants and their impact on the quality of the air are correlated exponentially. Although this method is easy to understand and straightforward, it ignores the evaluation indicators' synergistic effect. Ye et al. (2007) evaluated the underground air quality of uranium mines using the generalized contrastive weighted comprehensive scale index approach. Using generalized linear theory and fuzzy analytic hierarchy, Du et al. (2020) created a coal mine evaluation model where the generalized linear theory was used to analyze air, water, soil, and ecological compensation indicators to determine index factor relevance. Other authors (Dutta et al., 2004) in their work investigate the methods for the cumulative impact assessment of open-pit mining with a focus on air quality. Therefore, various methods presented in the researches, such as the substance-element model, pollution loss coefficient, generalized comparative weighted complex index approach, and generalized linear theory, expand our understanding and approaches to evaluating the quality of underground air, making an important contribution to this field.

It has been stated by Asif et al. (2018) that a variety of air quality models, including the box model, Gaussian model, Eulerian model, and Lagrangian model, are used to predict air quality for the mining sector. The authors developed the mining air dispersion model (MADM) for monitoring air pollution concentrations in open-pit mine regions. The model predicts the concentrations of six heavy metals (As, Pb, Hg, Cd, Zn, and Cr) as well as PM_{10}, $PM_{2.5}$ and NO_2 at different receptor locations. When the findings were compared to the monitoring field measurements, they showed a good degree of agreement for the target air pollutants, with R-squared values for $PM_{2.5}$, PM_{10}, and NO_2 ranging from 0.7 to 0.9, respectively. The analyses show that the air quality for the mining site can be systematically assessed using the algorithm given in this model. In another study conducted by Silvaster et al. (2009), the dispersion of mineral dust particles resulting from rock blasting activity in open pit quarry was analyzed using a computational fluid dynamics (CFD) model. The authors also mentioned that the CFD model can be applied to underground mining. PM concentration in the open pit copper mine has been measured and modeled in another study carried out by Patra et al. (2016b). For eight

days, measurements were made of the following meteorological parameters: wind speed, temperature, relative humidity, and PM concentration in seven size ranges: $PM_{0.23–0.3}$, $PM_{0.3–0.4}$, $PM_{0.4–0.5}$, $PM_{0.5–0.65}$, $PM_{0.65–0.8}$, $PM_{0.8–1}$, and $PM_{1–1.6}$. The correlation research demonstrated the relationship between depth and PM concentration as it moved from source to surface.

Significant emphasis should also be placed on the assessment of PM concentration in underground mining operations (Patra et al., 2016b). A number of studies used various measurement tools and methodologies to determine the concentration of PM in underground mines. In a study conducted by Saarikoski et al. (2019), an underground chrome mine revealed a significant influence of the location and time intervals of measurements on the number and mass concentration of particle matter. For measurements, an optical particle counter was used in various parts of the mine. It indicated that PM_{10} varied from 22 to 1100 μg/m^3, the total number of concentrations varied from 1.7×10^3 to 2.3×10^5 cm^{-3}, and the ore crushing process creates dust with particle sizes over 2.5 μm. At the same time, in the Saarikoski et al. (2018) study, the average concentrations of particles in a chrome mine were measured, and this value was $2.3 \pm 1.4 \times 10^4$ cm^{-3}. The distribution of the number of particles by size varied in the range from 30 to 200 nm, but the most common sizes were less than 30 nm. As an alternative for assessment, the properties of solid particles and aerosols in underground mining environments could be assessed by scanning electron microscopy and energy dispersive X-ray spectroscopy (SEM-EDS) analysis (Roy et al., 2015; Puławska et al., 2021; Akinyemi et al., 2022).

2.2 SEM-EDS analysis of PMs in underground mining

Another invaluable instrument for assessing the properties of PMs in underground mining environments is SEM-EDS analysis. According to Roy et al. (2015), SEM-EDS analysis enables the characterization of particle size, shape and morphology in the air, as well as the determination of the elemental and mineral composition of particles. Thus, the authors (Roy et al., 2015) conducted SEM analysis at a coal deposit in India and found the presence of soot, carbonaceous particles, and aluminosilicates at 9 out of the 18 stations examined. Significant findings at these sites include the presence of sizable crystalline particles linked to coal mining and flushing, as well as the occurrence of smaller particles generated by vehicular activity. While the X-ray analysis identified the existence of FeS_2, CuO, and $FeSO_4$ compounds over the research area, suggesting the possible influence of mining activities. Examples of SEM-EDS analysis are shown below in Figure 1.

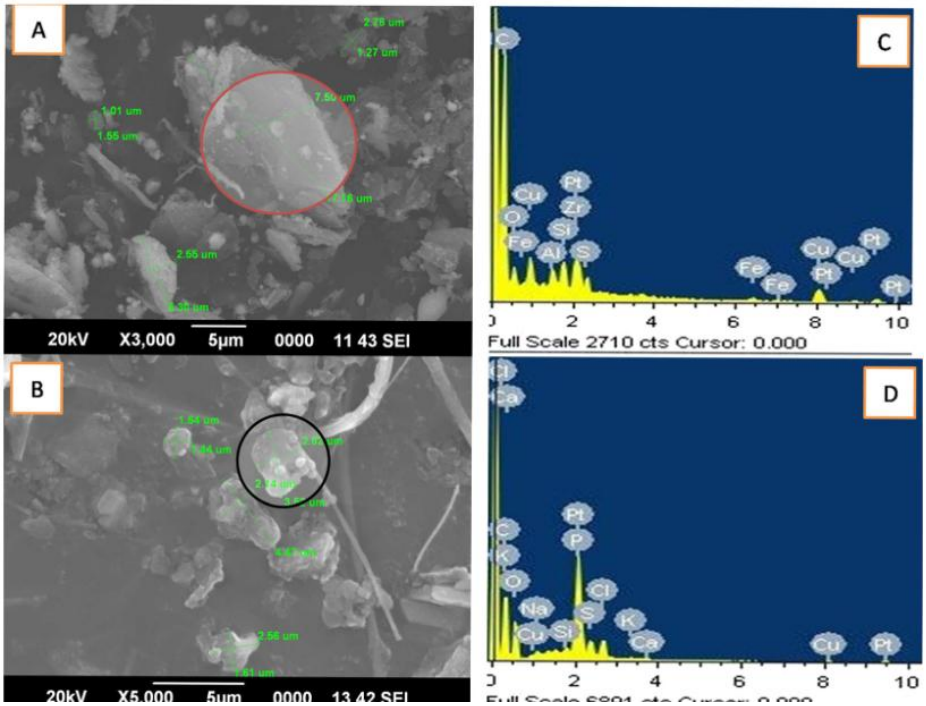

Figure 1. (A-D) SEM and EDS output of PM_{10} at different stations (Roy et al., 2015)

In one of the recent studies conducted by Azam et al. (2024), nano-sized coal dust particles in the Appalachian coal mining region were investigated and characterized through SEM-EDS analysis. Elemental analysis of these particles revealed significant levels of iron and silica, both of which have been linked to lung diseases when inhaled over long periods of time. Furthermore, a significant relationship between particle size and elemental composition has been discovered, emphasizing that smaller particles have a higher carbon content, whereas larger particles have higher concentrations of silicon dioxide and aluminum.

Therefore, SEM-EDS analysis can be helpful in examining and evaluating the properties of solid particles in underground mining. It can also be helpful in understanding of negative health effects of particles deposited in the alveolar region of the human respiratory tract. This can be accomplished through the utilization of an indicator such as the LDSA.

2.3 Lung Deposited Surface Area

The combustion of diesel is the main source of the toxic gases and particles in underground mines. When underground miners, particularly truck drivers, continuously breathe contaminated air for a prolonged period of time, severe occupational disorders may develop. In addition to toxic gases, diesel engines also release ultrafine particles (UFPs) with a size of less than 0.1 µm. Their accumulation in the respiratory system is hazardous and can result in severe

respiratory illnesses (Mine Safety and Health Administration, 2001). When evaluated in various environmental circumstances, the LDSA approach was successful in recognizing UFP (Afshar-Mohajer et al., 2020; Braakhuis et al., 2014; Kuula et al., 2020; Kuuluvainen et al., 2016; Huynh et al., 2018; Tran et al., 2020). Lepistö et al. (2023) characterise LDSA as the concentration of aerosols expected to deposit in the lungs after inhalation. LDSA measures the surface area of particles that collect in the alveoli of the human respiratory system. This metric is expressed in square micrometres (μm²). The authors assert that the particle type, particularly its composition and size, significantly influences this indication. Historically, there has been a lack of research about the quantification of this metric within the mining context.

Salo et al. (2021), using an electrical low-pressure impactor (ELPI+) in a chrome underground mine, found that LDSA concentrations vary from 137 to 405 $\mu m^2/cm^3$. The optimal particle size to estimate the LDSA distribution was no more than 100 nm, except at the blasting site, where the particle sizes were closer to 700 nm. Jafarigo et al. (2023) showed that the average concentration of LDSA was relatively high (4×10^3 $\mu m^2/cm^3$), while the majority of particles had a size of less than 100 nm. Afshar-Mohajer et al. (2020) monitored the concentration of inhaled particles in the four main technological divisions of a taconite mine, crushing, dry and wet milling, and granulation, to measure particles smaller than 300 nm. The results showed that the average LDSA concentration was highest during the granulation process, at 199 ± 48 $\mu m^2/cm^3$. In other mining areas, the concentration ranged from 80 to 200 $\mu m^2/cm^3$. In addition, the taconite mine LDSAs in crushing and pelletizing operations were 142 ± 52 $\mu m^2/cm^3$ and 200 ± 48 $\mu m^2/cm^3$, respectively.

UFPs can carry a high concentration of toxic substances, and therefore, they can cause inflammation through oxidative stress responses, atherosclerosis, an increase in blood pressure, and even myocardial infarction (Delfino et al., 2005). The LDSA is a different method of describing particle toxicity. The challenge with current mass-based exposure limits is that they fail to account for ultrafine particles (less than 100 nm), which have negligible contributions to particle mass but can penetrate deep into human airways, lodge in lung alveoli, and have high toxicity contributions. This is especially concerning because most diesel engine particle emissions (measured by number) fall into the ultrafine range (Braakhuis et al., 2014). In distinct metropolitan contexts, LDSA concentrations, size distributions, and height profiles have been measured in ambient conditions (Kuula et al., 2020; Kuuluvainen et al., 2016; Huynh et al., 2018). LDSA concentrations have been connected to emissions from combustion sources. Afshar-Mohajer et al. (2020) used a variety of measures, including LDSA, to investigate the

variability of aerosol concentrations in different processing zones of a taconite mine. Huynh et al. (2018) used numerous particle concentration measures, including LDSA, to investigate fine particle concentrations in six taconite mines. LDSA concentrations in their investigation ranged from 50 to 300 $\mu m^2/cm^{3,}$ depending on the processing region. Although LDSA levels varied from station to station, Afshar-Mohajer et al. (2020) also noticed the remarkable repeatability of concentration each day. This experimental sampling aimed to determine the exposure of the cabin operator to diesel exhaust nanoparticles.

Di Benedetto et al. (2010), in their study, were the first to characterize and determine the behavior of UFPs in synthetic lung fluids. The authors found large variability in the hydrodynamic diameter, with values less than 1 nm and greater than 5 μm, and recognized aggregation and disaggregation processes in Gamble solution and artificial lysosomal fluid using dynamic light scattering. The results of their study proposed an interaction between nanoparticles and lung fluids, particularly within the alveolar macrophage region (Schiavo et al., 2023). Kalaiarasan et al. (2024) concluded that respiratory deposition doses and particle number concentrations can be applicable to investigate relationships between particle diameter and deposition in the different regions of the lungs, considering the impact of the UFP deposition in the deeper region of the lungs.

A notable issue arises from the observation that a majority of the particles generated in coal and oil shale mines have a finely dispersed nature, enabling their infiltration into the respiratory system (Wang at al., 2019a; 2019b). Thus, the LDSA indicator can be used to determine the potential places of deposition of particles in the lungs and to study the impact of inhaled particles on humans (Lepistö et al., 2022). A number of researchers measured the LDSA in underground mines using a variety of measuring instruments in their research. Salo et al. (2021, 2023) studied the distribution and concentration of LDSA in various places of a chrome underground mine using an ELPI+ and evaluated the possibility of using sensors to measure this indicator. The author stated that the environment around the sensors was complex because the particle sizes often exceeded the optimal range (20–300 nm), and dust accumulated inside the devices. Studies conducted in different underground mines confirm the high concentration of fine particles. These results highlight the need for enhanced monitoring of mine air quality to protect workers' health and ensure safe working conditions. While understanding LDSA provides insights into respiratory interactions, examining the particle characteristics of oil shale and other air quality metrics allows for a deeper understanding of the properties crucial for their monitoring and measurement.

2.4 Diesel Particulate Matters

At present, diesel-powered equipment is one of the most crucial components in the field of underground mining operations, serving a vital function in extracting and transporting valuable resources. The majority of surface and underground mining operations, such as excavation, drilling, haulage, transportation and others, rely on diesel-powered equipment (Igogo et al., 2021). At the same time, the authors claim that one drawback of using diesel fuel is the emissions it produces – diesel exhaust particles. DPM was defined by Vouitsis et al. (2003) as a complex mixture of volatile organic and inorganic material added as exhaust gases cool down, as well as solid material (soot) created during combustion. According to Azam et al. (2024) and Khobragade et al. (2019), the DPM mostly includes fine particles of soot, hydrocarbons, sulfates and NO_x. Thus, exposure to particles with such a complex composition may lead to some occupational diseases.

DPM-related health issues are a very recent development in mining, having only started to surface in the late 1970s and early 1980s (Khan et al., 2021) The severe impacts of DPM exposure are recorded in published studies (Chang & Xu, 2017; Lee et al., 2015; Ristovski et al., 2012) with the chronic health effects of DPM exposure being of particular concern. Respiratory conditions, lung cancer, diminished lung function, pneumonia, and heart disease are among these health consequences (Chang & Xu, 2017). As stated in recent research conducted by Rumchev et al. (2020), underground miners may be exposed to DPM at a rate up to ten times higher than workers in other industries and diesel exhaust is regarded as a probable carcinogen. Typically, DPM contains around 40 carcinogens, as well as black carbon (BC) particles, which refers to a broad category of carbonaceous materials produced by incomplete fuel combustion in conditions of reduced or oxygen-free content (Shrestha et al., 2010). Approximately 90% of DPM is less than 1 μm (Jeong et al., 2021; Lim et al., 2021). Therefore, since diesel particles are smaller than respirable dust particles, they can penetrate deeply into the respiratory system (Braakhuis et al., 2014). Several studies have confirmed the risk of accumulation and deposition of diesel particles in the human body. For example, DPM was categorized as human carcinogenic by the International Agency for Research on Cancer (IARC) because of adequate evidence from animal and epidemiological research (Chang & Xu, 2017). In another study reviewing the impact of DPM on health, more than 12,000 mineworkers who are exposed to DPM emissions at eight non-metal mines in the United States were chosen from among underground miners (Turner, 2007). According to the study's findings, the average DPM concentrations for workers on the surface and those working below ground were 1.7 and 128.2

$\mu g/m^3$, respectively. In general, the data collected during the study showed that the group exposed to high concentrations of DPM (miners working underground) has a higher risk of death from lung cancer than the group exposed to low concentrations (miners working on the surface). This study concluded that as the duration of exposure to DPM increased, the data indicated a tendency to increase the risk factors for lung cancer mortality. The above-mentioned pieces of evidence point to detrimental effects for workers exposed to diesel particulates, which indicates the necessity for careful DPM monitoring present in the mining work area.

DPM monitoring methods are comparatively new in the mining industry, and techniques that can evaluate real-time DPM in underground mines are still developing. For DPM measuring, certain commercially available aerosol monitors or particle counters are commonly employed, utilising the real-time light scattering principle (Arnorr et al., 2008). Nevertheless, these devices are not specifically designed for DPM measurements in compliance with regulatory requirements (Pinssar, 2023). In order to ensure compliance, the majority of mining companies employ the widely recognized NIOSH 5040 standard as the most precise approach for assessing the long-term effects of DPM on workers (Schauer, 2003). Volkwein et al. (2017) highlight the significant advantage of this method because it reduces the likelihood of measurement results being influenced by mineral sources or other flammable substances. Additionally, it allows for the differentiation of carbon content into organic carbon (OC) and elemental carbon (EC) components to calculate a total carbon (TC) value (Birch & Noll, 2004). However, despite its advantages, this approach is hindered by some drawbacks, such as the time-consuming nature and the imprecision in capturing particles (Koponen et al., 2023). The temporal lag in the first case is caused by the requirement to process the outcomes in a specialized distant research laboratory. The second case has a disadvantage in that it is unable to identify temporary but significant increases in DPM levels. So, the NIOSH 5040 approach is inherently incapable of detecting DPM transients during the measuring process (Khan et al., 2021). Nevertheless, real-time assessment of DPM is still highly significant because it facilitates the assessment of prevailing conditions and allows for a more rapid assessment of DPM management solutions.

However, an ongoing debate has emerged regarding the most appropriate metric for quantifying DPM. According to Bond et al. (2013), the environmental community usually uses black carbon as a metric, while Noll et al. (2006) report that the mining sector utilises elemental carbon as their measurement. These two concepts exhibit a high degree of similarity, but the only clear difference appears to be the sophistication of the analysis. Simultaneously, there are a number of studies that demonstrate the relationship of BC to total carbon, elemental carbon and DPM.

For example, Fruin et al. (2004) examined the impact of BC in automobiles as a measure of DPM effects in California. They found that the exposure to BC was 4 μg m^{-3}, which is equivalent to DPM concentrations ranging from 7-23 μg m^{-3}. Additionally, the study revealed that the conversion factor for transforming BC into DPM ranges from 1.8 to 5.6. In comparison with this, Burtscher et al. (1998) demonstrated that the proportion of BC to the overall quantity of DPM collected from the tailpipe varied between 45% and 100%. In another study (Barrett et al., 2019) that evaluated various DPM field monitors for underground mining applications, the AE33 Aethalometer (AE33) measurements revealed that the ratio of BC to EC is approximately 2.0 at low concentrations and around 1.5 at higher concentrations. Similar results were obtained in a study by Volkwein et al. (2017) on the measurement of DPM in a large underground metal mining mine. The average levels of BC were below 53 μg/m^3. Additionally, there were distinct patterns seen in BC levels that corresponded to shifts, shotcrete loading times in the drift and blasting activity. Finally, the researchers discovered that the concentration of black carbon is approximately twice the concentration of elemental carbon (BC=2×EC). Volkwein et al. (2017) in another study on the use of an environmental "black carbon" particle sensor AE33 to measure DPM in three underground mines stated that the proportion between BC and EC was approximately 1.5 (BC=1.5×EC). Additionally, a ratio of 1.7 between BC and EC was found in a study on the assessment of a sensor for continuous monitoring of diesel particulate matter in mines to optimise the ventilation system of the mine (Volkwein et al., 2016). According to a recent study conducted by Koponen et al. (2023) on the use of aethalometers to measure the concentration of DPM in underground mines, the average ratio of black carbon to elemental carbon was found to be 2.1±0.7 (for AE33) and 2.4±1.7 (for MA200). Finally, it should be emphasized that different studies demonstrate a considerable relationship between black and elemental carbon for quantifying DPM, however, their utilization may vary by the specifics of the industry. It may also be beneficial to study the relationships between other air quality indicators for further analysis of PMs in an operational mining environment.

2.5 The relationship between air quality metrics

The significant impact of air quality on the health of miners in underground mines has led to a growing interest in studying air quality indicators. Some important air quality indicators include PMs, LDSA, PNC, BC and average particle diameters. Each of these indicators reflects a certain aspect of the properties of pollutants. Understanding how these indicators relate to each other

is important for a thorough assessment of air quality, as these indicators often interact and affect health conditions, especially cardiovascular and respiratory diseases.

While there is a lack of research into LDSA in the mining sector, several research papers have examined this important indicator in urban environments. A study conducted by Mukherjee et al. (2024) to investigate the impact of an electrostatic precipitator on the emission of BC and particle lung-deposited surface area from residential wood combustion in Finland found that the contribution of BC to LDSA varies depending on the combustion phase. Thus, BC is the primary contributor to LDSA in the flaming phase. Previously, Kuula et al. (2020) noted a high correlation (> 0.50) between BC and LDSA in work on investigating the long-term exposure to lung-deposited surface area (LDSA) of particulate matter (PM) from various sources in Finland. Lepisto et al. (2022) also described a high correlation between the two parameters (0.92-0.97) in their article on the relationship between LDSA and BC levels in road and harbour environments in Finland. The high correlation between the two parameters ($r = 0.84$) is further supported by a study conducted in Finland, focused on developing a new statistical model to estimate LDSA concentrations (Fung et al., 2022).

Furthermore, it is essential to examine the relationship between LDSA and particle size since this may be crucial for comprehending the behavior of particles of differing sizes when inhaled and deposited within the respiratory system. In one article focused on the distribution of sizes of particles that deposit in the lungs in various urban environments in Finland, Kuuluvainen et al. (2016) found that the LDSA concentration correlates well with the mass of small particles, namely $PM_{2.5}$. A high correlation between LDSA and $PM_{2.5}$ is also supported by a study conducted in Finland, focused on developing a new statistical model to estimate LDSA concentrations (Fung et al., 2022). In this study, the correlation coefficient was approximately 0.8, indicating a strong dependence between the two indicators. In addition to $PM_{2.5}$, the highest correlation in this study was observed between LDSA and BC, reaching approximately 0.84. In another article which was conducted in Spain and dedicated to understanding the factors that influence the number of airborne particles that settle in the lungs, authors compared data on the BC, the total particle number concentration and the particle size distribution with the LDSA (Reche et al., 2015). This study indicates that particles sized between 50 and 200 nm predominantly influence LDSA concentrations. This range of particle sizes showed the strongest correlation ($r = 0.78$) between LDSA and PNC (Hama et al., 2017). More recent studies aimed at examining the sources of PMs in urban area of Taiwan and the associated

health risks have confirmed the above-described results. Thus, Chang et al. (2022) discovered that between $PNC_{50–200}$ and LDSA had the highest correlation coefficient among all size ranges.

The relationship between BC, particle size, and concentration may be of interest to researchers since it gives information about the physical and chemical properties of aerosols. Gramsch et al. (2014) in a study aimed at analyzing the influence of particle size on black carbon pollution levels in the atmosphere of Santiago, found that BC is mainly associated with larger particles (175-700 nm), and the correlation decreases with decreasing particle size ($r < 0.4$). At the same time, Betancourt et al. (2017) found a correlation between particulate matter with a diameter of less than 2.5 microns ($PM_{2.5}$) and BC in another study that investigated the amounts of air pollutants in different transportation microenvironments in Colombia. In a study examining the association between air pollution and blood pressure in a population living near highways in Boston, the results showed that $PM_{2.5}$ and BC had a strong correlation ($r = 0.79$), whereas PNC had a weak correlation ($r = -0.01$ for $PM_{2.5}$ and $r = 0.30$ for BC) with the other two indicators (Chung et al., 2015). Thus, for a complete understanding of the impact of PMs on air quality in the operation of mining enterprises, it is necessary not only to study the relationship between various air quality indicators but also to examine in detail the characteristics of the particles themselves, particularly the particles of oil shales.

2.6 Oil Shale Particulates

Nowadays, increased attention is received to PMs in underground mines since their concentration is a key aspect of the health and safety of workers. According to Wang and Liu (2022), and Gratt (1985), coal and oil shale mines are significant sources of dust particles in the mining environment, and their detailed study in the context of composition, size and monitoring methods is of particular interest. For example, in coal underground mines, dust includes the smallest particles and this dust consists mainly of coal particles containing carbon, heavy metals (arsenic, mercury, lead, etc.) and other pollutants that can lead to serious diseases of the respiratory tract of mine workers (Liu & Liu, 2022; Chang & Xu, 2017). Moreover, Widodo et al. (2023) claim that in coal mines, especially with improper ventilation, the formation of explosive mixtures of dust and gas is possible, which increases the risk to workers. According to Zhang et al. (2021), 60-80% of all coal dust is usually generated in mining operational faces. In addition, the concentration of coal dust there can reach more than 3000 mg/m^3 (Chen et al., 2018), which significantly exceeds the permissible concentration of total dust of 4 mg/m^3 specified in the Safety Regulations for Coal mines. Another study on the measurement of dust

concentration in a coal underground mine conducted by Jin et al. (2023) showed that it ranges from 3.4 to 106.2 mg/m^3.

In comparison with coal mines, oil shale mines produce dust with a different composition (Wang et al., 2019a; 2019b). According to the authors' study, oil shale dust contains minerals such as quartz, gypsum, and mica, as well as various chemical compounds associated with oil and gas production processes (kerogen, lead, cadmium, etc.). Typical oil shale mineral parts chemical composition consists of SiO_2, Al_2O_3, Fe_2O_3, TiO_2, CaO, MgO, SO_3, K_2O, Na_2O, P_2O_5, and kerogen oil with an elemental composition H, C, S, N, and O (Dyni, 2016; Sabanov et al., 2023). As an unconventional resource, oil shale is widely distributed around the world and has a very high potential; however, industrial mining produces it only in China, Estonia, and Brazil (Dyni, 2016; Sabanov et al., 2023). For this reason, there are only a few studies related to oil shale dust compounds, and none about particulate matter or aerosol concentration and distribution in oil shale underground mines. Wang et al. (2019a), in their study about the explosibility of oil shale dust, argued that dust particles in oil shale have an extremely small size and fine dispersion. In the study of kinetic analysis on the deflagration characteristics of oil shale dust conducted by Meng et al. (2022), the distribution of particles of oil shale dust was determined using a laser particle size analyzer called 'Mastersizer 2000'. So, Figure 2 shows the results of two different measurements. The average particle size of two different oil shales was 15 μm and 60 μm, respectively. For oil shale with a particle size of 15 μm, the average diameter is approximately 5 μm, and the average volumetric diameter is about 30 μm. In the case of oil shale with a particle size of 60 microns, the average diameter is around 27 μm, and the average volumetric diameter is about 63 μm.

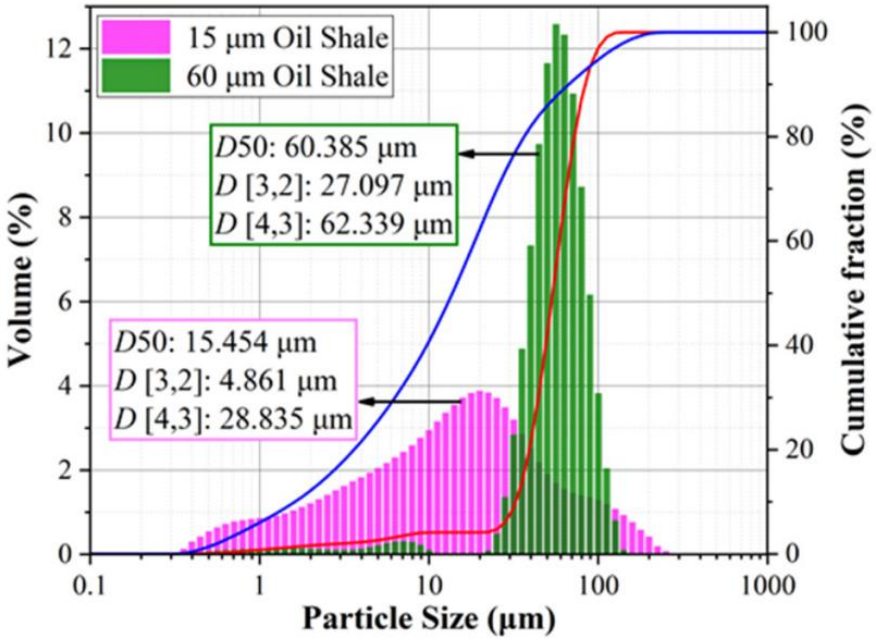

Figure 2. Particle size distribution of oil shale dust (Meng et al., 2022)

However, studies conducted by Yu et al. (2017) on the measurement of oil shale dust particles selected in the four main areas of oil shale extraction have shown different results (Figure 3). The particle sizes in the oil shale dust were measured using a laser diffraction analyzer with particle sizes 68–80 μm. In a study by another author (Teinemaa et al., 2002) on an investigation of oil shale combustion fly-ash aerosols, it was stated that the bimodal composition first maximum at 0.1 μm (fine particles) and a second maximum around 3.5 μm (coarse particles). Moreover, during the experiment, the inhaled particle fraction increased from 25% to 65%.

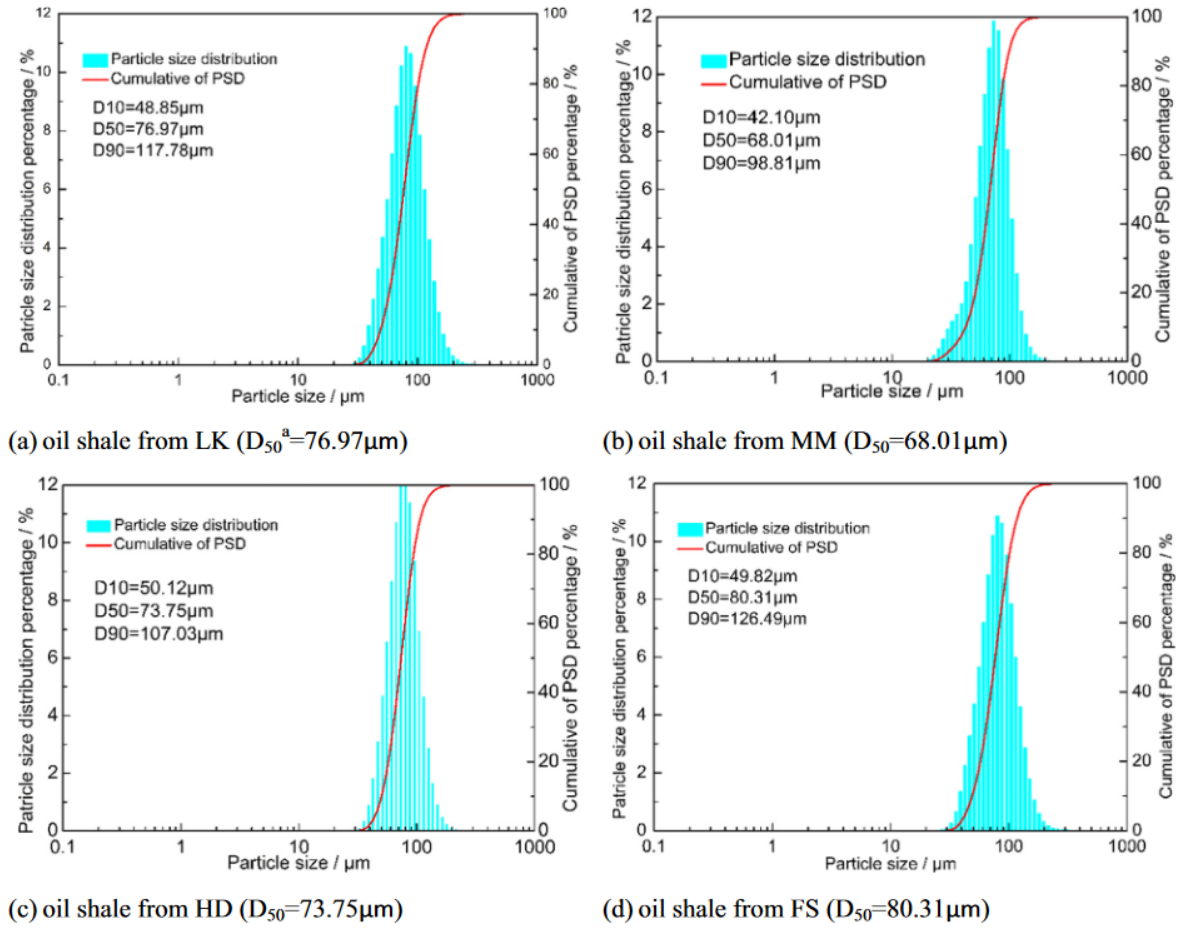

Figure 3. Particle size distributions of oil shale dust samples (Yu et al., 2017)

However, all of these studies on oil shale were limited to measurements, monitoring, and analysis of PM and LDSA in underground oil shale mines, and therefore focused on the air quality problems in operational faces. The aim of this study is to analyse PM and LDSA concentrations in the operational workings of the oil shale underground mine. Producing relationships between currently used PM indicators and more descriptive and innovative indicators (LDSA and PNC) determines the need to study these components. The investigation of the correlation between LDSA and PM_1 and $PM_{2.5}$ is an important part of this study because these indicators have more diverse sources, including diesel exhaust emissions and secondary aerosol formation, which might be anthropogenic or biogenic in origin (Sillanpää et al., 2022). Kuula et al. (2020) and Luoma et al. (2021) stated in their studies that $PM_{2.5}$ has been shown to highly correlate with BC and LDSA (Kuula et al., 2020; Luoma et al., 2021). PM_{10} concentrations are dominated by noncombustion sources, e.g., dust.

This paper begins with a brief overview of the mine site and a description of measuring instruments, introduces results, and leads to a discussion. Measurement results include filter

analysis by SEM/EDS, simulation results visualized as a particle concentration distribution and derived relationships between LDSA and PM. This study offers important data on PM and LDSA exposure to miners at various working operations in the oil shale mines, and therefore can be used to optimize auxiliary ventilation to dilute toxic concentrations. Such experimental measurements of PM and LDSA have never been conducted at any underground oil shale mines; thus, the produced analysis and received results will considerably contribute to the development of wide global knowledge in this field. These findings enhance our understanding of the different particle concentrations and should help devise ways of reducing exposure to miners, as well as estimating the risks associated with the health of workers in hazardous areas. From an innovation perspective, the exposure limits should be represented by nanoparticles, and LDSA can be an option to use as a measure to demonstrate health relevance.

3. METHODOLOGY

3.1 Study Mine Site

The study mine, located in Estonia, operates at a depth of 50 meters and employs the room-and-pillar mining method with drilling and blasting, followed by mucking to conveyors, which transport the oil shale to a beneficiation plant with an annual production of 6 million tons. Two operators were assigned to a single Load-Haul-Dump (LHD) machine, which had the highest diesel emissions impact on the mine's ventilation system. In addition to the LHD operators, the workforce included three firemen working across two shifts. One miner per shift was responsible for operating the drilling jumbo and performing roof support tasks. Furthermore, two operators were allocated specifically for large-diameter hole drilling. The studied mining block dimensions are about 300 m in width and around 800 m in length, located at a depth of 50 m (Figure 4). The dimensions of the pillars are about 50 m^2. The room's size is about 7 m by 7 m. In this study, samplings were produced at three location points: Zone 1 (black star) is on the incoming fresh airflow, Zone 2 (purple star) is on the operational face, and Zone 3 (red star) is on the dumping point (8-point green star) to the conveyor belt (Figure 4). In Figure 4, blue arrows show fresh air and red arrows present exhausted air; the green seven-point star is a dumping station; and the grey line in the middle of the mining block is the belt conveyor.

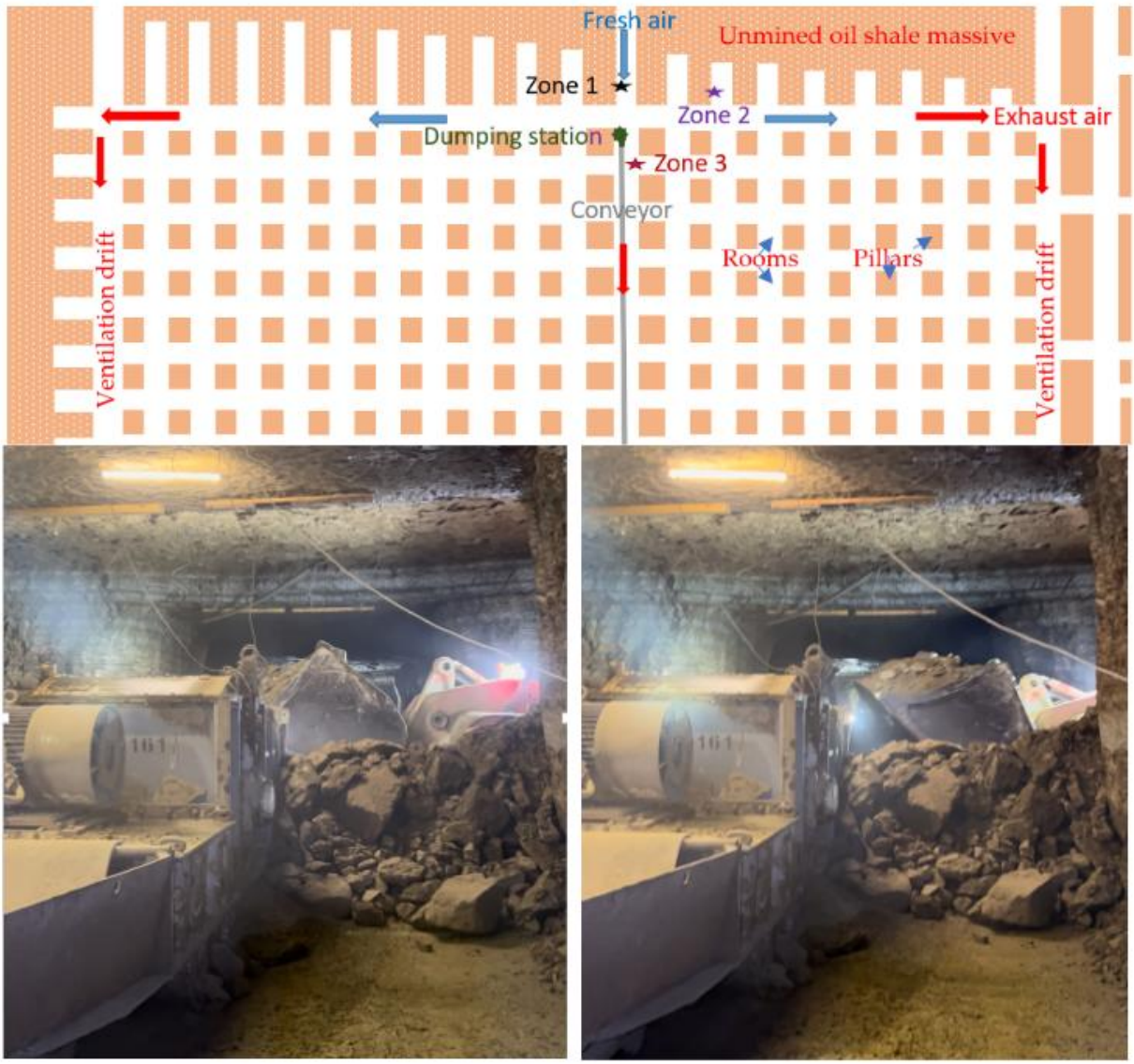

Figure 4. Schematic layout of the measurement area in the underground mine using the room-and-pillar mining method, and photos from the dumping station with the loader bucket taken by the authors

The studied oil shale is made of organically rich stratified sedimentary rock (15–46% kerogen, 26–57% carbonates, and 18–42% clastic minerals). The karst clay composition is approximately 10–15% within tectonic displacement zones. The fractured zones' rock is dolomitized and contains calcite and pyrite veins, as well as marcasite, galena, sphalerite, and barite. The mined oil shale seam comprises thin layers of oil shale together with thin intervening layers of limestone. Oil shale uniaxial compressive strength is 18–40 MPa, and limestone is 65–82 MPa; the volume density varies from 1.2 to 1.7 t/m^3 and from 2.1 to 2.5 t/m^3, respectively (Sabanov et al., 2023a; Sabanov et al., 2023b). The average chemical composition of the oil shale mineral part is presented in Figure 5.

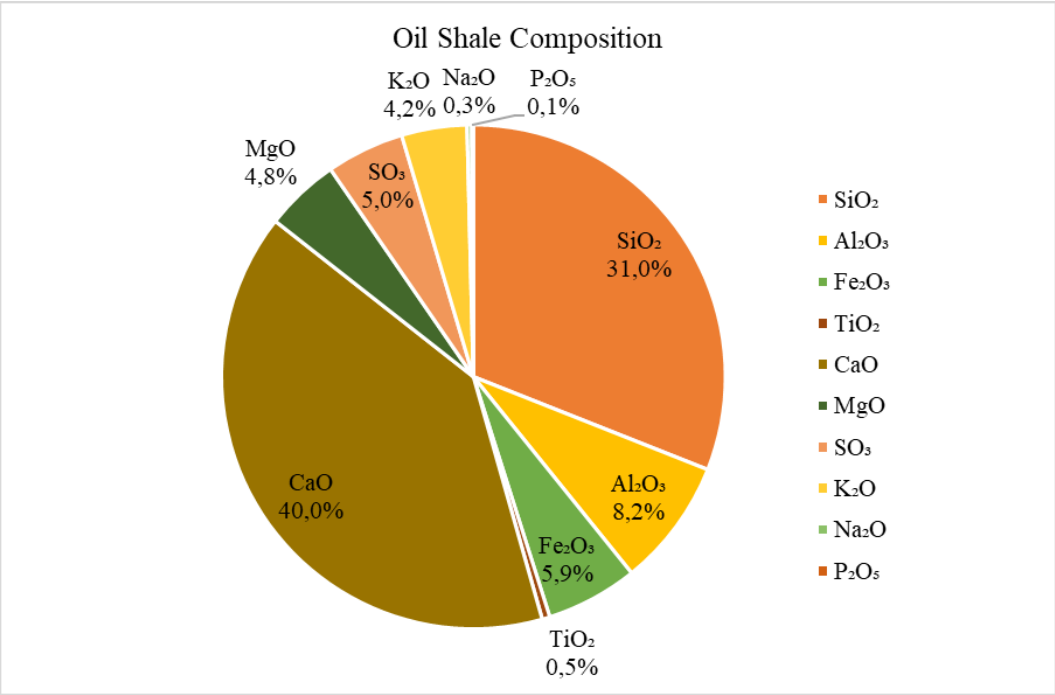

Figure 5. Chemical composition of oil shale mineral part

The entire operation of the mine's ventilation system is facilitated by the utilization of intake ventilation fans, each with an airflow rate of 140 m^3/s. These fans are situated on the surface and are responsible for supplying fresh air to the operational sections of the mine. Additionally, booster fans are installed underground to assist in this process. The polluted air is circulated through exhaust ventilation tunnels and released to the surface through return ventilation shafts (Sabanov, 2018). The sampling instruments were placed 160 cm above the floor to ensure effective collection of samples near the mineworker's respiratory level. The experimental measurements were conducted in Zone 2 and Zone 3 (Figure 4), requiring the use of the LHD loader 'Liebher LH410' with a bucket size of 6.5 m^3 and equipped with the diesel engine model 'Volvo TAD872VE, 210 kW, Tier 4f'. The loader exploits high-quality diesel fuel to meet Euro 3 standards, and at the moment of measurements, the engine hours were 15, 835 eng/h. Samplings were conducted at a working engine temperature of 90 ˚C, which was in operation for 2 h without stopping. In Zone 2, the sampling was produced about 2 m away from the loader exhaust tailpipe to consider diesel particulate matter (DPM) emissions. In Zone 3, samplings considered a process of oil shale dumping from the loader to the conveyor, which is associated with a high-dust environment where diesel emissions are also present. In Zone 3, the sampling point was about 8 m away from the loader. All measurements were produced on the downstream air, whose quantity was about 20 m^3/s. The mine environment conditions obtained from the

instruments showed that the air temperature was 12 °C, the humidity was 87%, and the atmospheric pressure was 1024 hPa.

3.2 Measuring Instruments

The 'Naneos Partector 2' (Naneos Particle Solutions gmbh, Alte Spinnerei 9, CH-5210 Windisch, Switzerland) multimetric particle detector uses dual noncontact detection stages to measure the LDSA, PNC, and average particle diameter (d). Additionally, it calculates the particle surface area concentration (SA) and the particle mass < 0.3 μm ($PM_{0.3}$). The manufacturer provides the following measurements and accuracy ranges for each variable of Partector 2: LDSA = 0–12,000 ± 30% $\mu m^2/cm^3$, SA = 0–50,000 ± 30% $\mu m^2/cm^3$, d = 10–300 ± 30% nm, PNC = 0–106 ± 30% pt/cm^3, and $PM_{0.3}$ = 0–1000 ± 50% $\mu g/m^3$. The displayed LDSA value is only accurate in the size range of 20–400 nm; however, the instrument can be used to measure micron-sized particles too. The 20–150 nm uses a fixed deposition voltage, and the 10–300 nm uses an adaptive deposition voltage. The particle size range of LDSA is from 10 nm to 10 μm, and for size distribution, it has 8 channels between 10 and 300 nm. The noise floor is about 0.5 $\mu m^2/cm^3$ in particle-free air for LDSA.

Partector 2 uses diffusion charging of airborne particles, and the resulting measurement of acquired particle charge is used to compute LDSA, and from this metric, to estimate particle number and particle size. When there is a temporal charge gradient in the induction stage, a current spike is induced with a magnitude proportional to the charge gradient. The total current induced by particle-borne charges is determined from the current peaks in the induction stage, and the alveolar LDSA concentration is determined by applying a corresponding calibration factor (Salo et al., 2021; Todea et al., 2015; Fierz et al., 2014). The instrument achieves a resolution of 1 s for particles larger than 10 nm. Partector 2 comprises a unipolar emission charger, an ion trap, and an induction stage for detecting the particle charge. The flow rate of the sample was 0.5 L per minute.

For PM concentrations, the 'DustTrak™ DRX Aerosol Monitor 8533' (TSI Incorporated, 500 Cardigan Road, Shoreview, MN, USA) was used to simultaneously measure both mass and size fractions of aerosols. The DustTrak is a 90° light scattering instrument that measures both particulate size fraction (PM_1, $PM_{2.5}$, PM_4, PM_{10}) and mass concentration, and allows real-time aerosol monitoring. The mass concentration range is from 0.001 to 150 mg/m^3, with an accuracy of ±5%, and the particle size range is 0.1–15 μm (Kappelt et al., 2023). During the sampling, the DustTrak pump flow rate was set at 1.7 L per minute (lpm). The DustTrak was equipped

with a 37 mm replaceable mesh filter inside the concealed filter kit within the body. The mesh filter sample was used to analyze the morphology and elemental characteristics of airborne particles under the scanning electron microscope (SEM) 'Jeol JSM-IT200' (JEOL, Freising, Germany) integrated with energy dispersive X-ray spectroscopy (EDS). The sputter coating layer of 5 mm thickness was applied to the sample filter and then placed inside the SEM for analysis. The desktop computer connected to the SEM contained the application 'SEM Operation'. This computer program was used to control all aspects of the equipment. Moreover, the experimental data collected from the field and the laboratory experiments were analyzed using a single variable regression approach. The R-squared value was what determined the strength of the correlations between the variables. The SEM/EDS examination of individual particles yields crucial data regarding the size, shape, quantity, elemental composition, and surface area of the particles. This information is valuable for conducting a comprehensive physicochemical characterization of PM in order to investigate particle deposition and toxicity. The JSM-IT200 is equipped with functionalities that allow for efficient and effortless SEM investigation. With an accelerating voltage of 30 kV, the electron optics system can reach a resolution of 3.0 nm. It is very flexible and can be used for everything from high-resolution observation to EDS analysis. The Specimen Exchange Navi is a user-friendly feature that provides guidance for tasks such as sample loading, area search, and SEM image viewing. The EDS system is fully integrated and consists of a silicon-drift detector with a resolution of 130 eV. It also contains a feature called "live EDS Analysis", which allows for the simultaneous presentation of the chemical composition of the specimen while imaging. The "Zeromag" function simplifies sample navigation, making it easier to focus on research points on the sample. The length, width, and height of the sample size are limited to 3 cm × 3 cm × 2 cm, respectively (Balasurya et al., 2020; Fatima et al., 2023).

3.3 Data Analysis Tools

Regression analysis is employed to examine the impact of independent variables on dependent variables, and to compute the numerical values of the dependent variables (Duan et al., 2017). Based on the quantity of independent variables and the data analysis conducted in this experiment, single-variable linear regression and nonlinear power regression models were adopted. The mathematical representation of the linear regression model is as follows:

$$y = mx + b \tag{3}$$

where y is the dependent variable, x is the independent variable, m is the estimated slope, and b is the estimated intercept. The mathematical expression of the nonlinear power regression model is as follows:

$$Y = ax^b \tag{4}$$

where y is the dependent variable, x is the independent variable, and a and b are constants determined by the regression analysis.

The coefficient of determination R^2 is used to measure the quality of the fit in regression analysis. The number of variables refers to the proportion of the dependent variables' variability that is explained by the regression equation. It is one of the measures used to assess the adequacy of the fit (Jose et al., 2015). The coefficient of determination, R^2, varies between 0 and 1, with a higher R^2 number indicating a stronger correlation. The R^2 can be calculated as follows:

$$R^2 = [1 - SSR/SST] \tag{5}$$

where SSR is the sum of squared regression, and SST is the total sum of squares, the distance of the data away from mean all squared (Galoie et al., 2023). Monte Carlo simulation is used for building models demonstrating possible outcomes of LDSA and PM_1 at Zone 2 and Zone 3 by considering the instrument's accuracy. The distribution of probability, which is a range of values, replaces any uncertainty factor when producing the models. After that, numerous computations of the outcomes are produced, at every turn establishing a variety of stochastic variables for the probability functions. Monte Carlo modeling helps to determine the value distribution of the probable numbers with several likely outcome values. For this study, Monte Carlo modeling uses input results from the program evaluation and review technique (PERT) distributions (Clark, 1962; Lambrigger et al., 2009; Karwański & Grzybowska, 2018). Palisade@Risk 8.5 software is used for Monte Carlo modeling. The Weibull distribution for fit comparison of LDSA and PM values for each location of the measurements is proposed (Fung et al., 2022).

3.4 Ventsim Software Simulation

Ventsim program allows for creating three-dimensional models of mines, analysis of airflow movement, calculation of particle concentrations, and optimization of ventilation systems (Maleki et al., 2018). In this study, the Ventsim software was used to model the distribution of diesel particles and dust in an underground oil shale mine.

The mine model (Figure 6) was constructed using information previously provided in the study mine site section on the geometry of mine workings, ventilation unit locations, and pollution sources (Figure 4). Fans, ventilation shafts, the main workings, and other components were all included in the model. The dumping station and upper face, where the diesel equipment was in operation, were the source of the dust and diesel particles. Data with concentrations of DPM and dust in pollution sources, which were measured by instruments during the study, were added to the software. The values of $PM_{0.3}$ measurements were taken for the DPM concentration, and PM_{total} values were taken for the dust concentration. Airflow data was also incorporated, as this parameter affects the dispersion rate of air pollutants. The airflow for the intake ventilation fan was specified as 140 m^3/s. The vehicle settings were modified. Two diesel equipment units were incorporated into the modelled mine areas: LHD loader working in the working face and the dumping station to simulate the operational conditions. This allows for the specification of speed and aerodynamic characteristics of the vehicles.

After entering all parameters into the software, a dynamic or contaminant simulation was performed. Contaminant simulation involves steady-state modeling of pollutants based on model data. The simulation offers several types of pollutant modeling (contaminant, diesel, gas, dust, and others). This simulation distributes pollutants from sources throughout the model as a continuous, uninterrupted flow. Color markings automatically switch to indicate pollutant concentration, displaying the simulated dispersion and degree of contamination.

Two types of simulations were performed: a diesel simulation for DPM and a gas simulation for dust. Firstly, the dispersion of DPM was simulated based on diesel sources within the mine model. The result is displayed as a concentration per unit volume of airflow. Diesel sources are converted into DPM emission rates per unit engine power, based on either default or custom settings. Diesel emissions are distributed throughout the model using a steady-state complete mixing algorithm, which assumes ideal mixing and no particle settling (Ventsim Design User Guide). It is assumed that diesel emissions accumulate, and subsequent sources or recirculation can increase the concentration beyond the initial source. Subsequently, a gas simulation for dust was conducted. Gas simulation is based on the same linear distribution algorithm as other contaminant simulations. The simulation was performed for time intervals of 30 minutes, 1 hour, 3 hours and 6 hours. This allowed for the evaluation of particle distribution dynamics over time. To view the dynamic simulation results, so-called "monitors" were placed into the model. The simulation results are displayed on a graph in dynamic mode as the simulation

progresses. The simulation results were visualized as particle concentration distribution maps in the Results section (Figures 19 - 22).

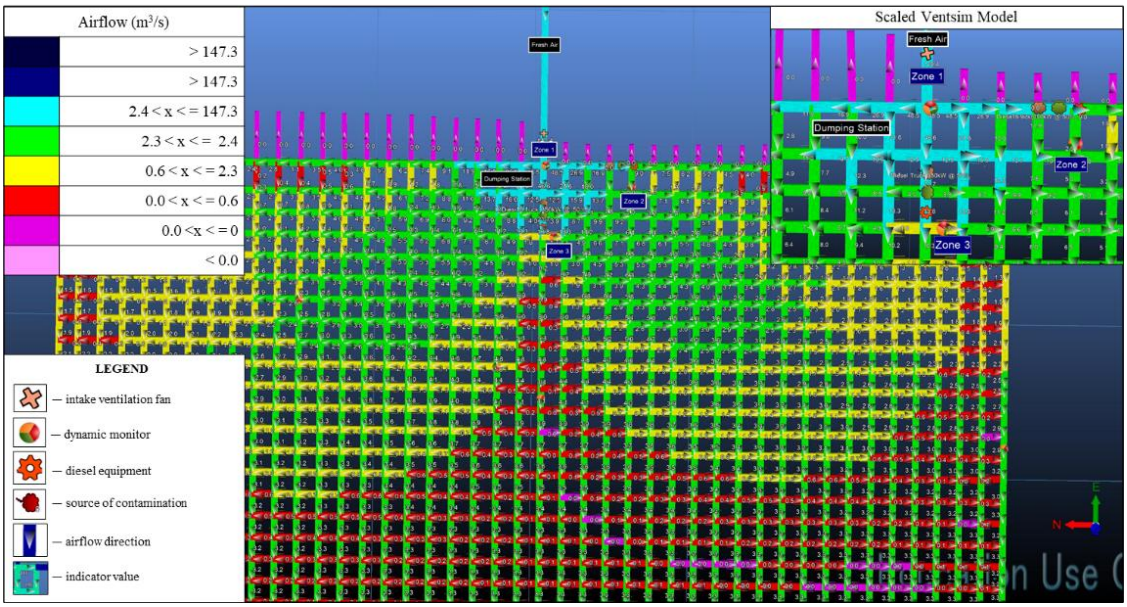

Figure 6. Schematic Ventsim airflow (m^3/s) model of the working area of a study underground oil shale mine

In comparison with CFD, which allows for more detailed and realistic modeling of emission distribution by capturing complex fluid behavior and fine-scale turbulence, Ventsim Simulation is still remains a useful tool for simplified modeling of airflow and pollutant dispersion in mine ventilation systems. Ventsim has a more user-friendly interface, faster computation speeds, and requires substantially fewer computer resources and specialist skills than CFD. These qualities make it ideal for realistic, large-scale ventilation planning, as in our case, preliminary assessments, and real-time scenario testing in mining situations, where quick decision-making and accessibility are critical (Wang et al., 2019b; Ventsim Design User Guide).

4. RESULTS

4.1 Measurements Results

The analysis was based on data from our previously published work (Sabanov et al., 2024). Figure 7 demonstrates the measurement results of PM, LDSA, SA, PNC, and diameter in three zones.

In Zone 1, measurements were produced over 217 s with a sampling interval of 1 min. All PM_1 and $PM_{2.5}$ showed nearly close values; however, PM_{10} and PM_{total} have peaks because of some disturbance from other mine activities (opening and closing air doors, diesel vehicles, etc.). $PM_{0.3}$ measured by the Partector is similar to the averaged PM_1, but the curve has some drops contradictory to the peaks of PM_{total}. However, LDSA and PNC were stable apart from those external disturbances. Surface area concentration has similar drops compared to $PM_{0.3}$ readings, as the same instrument, Partector 2' produced it.

In Zone 2, the instruments were placed in the operational room (Figure 1) for a total sampling time of 356 s, but only for 150 s did the loader produce its work in the face. This was done for safety reasons: leave instruments alone in the mine's working face and do not restrict the loader's maneuvers and work. PM has peaks at the time of 80 s and 210 s when the loader entered and exited the room. These peaks can be interpreted as oil shale dust. Then, the loader's diesel engine was running at its nominal working rate of 2300 RPM (revolutions per minute) to produce the highest diesel emission concentration that can be used to estimate DPM. This can be observed in Figure 6, Zone 2, where peaks of LDSA and PNC appeared on the interval from 95 to 203 s. At the same time, the particle diameter dropped.

In Zone 3, the instruments were allocated to the downstream air, about 8 m away from the dumping point where the oil shale material was dumped on the conveyor. The total sampling duration was 424 s with four dumping cycles, whose peaks (about 2–7 s per dump) can be seen in Figure 4, Zone 3. Dumping was carried out on the time interval of 62–67 s, 115–118 s, 178–181 s, and 337–341 s. Between the peaks, the LDSA and the PNC were not too different from the regular mine air atmosphere in comparison with the incoming fresh air measurements in Zone 1, thanks to the sufficient mine ventilation.

Tables 1 and 2 below present measurement data statistics showing minimum, mean, and maximum values. Full descriptive statistics are presented in Tables 3 – 8. In Zone 3, all PM is very high compared to Zone 2. Zone 3 minimum PM numbers are very close to each other;

however, maximum values differ considerably due to dumping peaks associated with high dust dispersions. However, Zone 2 has the highest maximum values for the LDSA, the surface area, and the PNC.

Table 1. Measurement data basic statistics (Partector 2). Adapted from Sabanov et al. (2024)

Name	Value	Zone 1	Zone 2	Zone 3
LDSA (µm²/cm³)	min	112	142	161
	mean	125	554	372
	max	136	2251	1848
	STDV	0.30	32.60	12.11
Surface Area (µm²/cm³)	min	501	744	1036
	mean	1028	3246	2426
	max	1191	1.42×10^4	1.17×10^4
	STDV	7.06	152.92	72.41
PNC (pt/cm³)	min	2.62×10^4	2.26×10^4	2.49×10^4
	mean	3.44×10^4	2.48×10^5	1.39×10^5
	max	6.88×10^4	9.63×10^5	9.25×10^5
	STDV	413	1.80×10^4	5669
Diameter (nm)	min	32	28	30
	mean	65	59	54
	max	77	150	150
	STDV	0.49	0.84	0.61
$PM_{0.3}$ (µg/m³)	min	9	15	25
	mean	38	89	70
	max	51	475	369
	STDV	0.47	3.24	1.98

Table 2. Measurement data basic statistics (DustTrak). Adapted from Sabanov et al. (2024)

Name	Value	Zone 1	Zone 2	Zone 3
PM_1 (µg/m³)	min	44	95	124
	mean	48	190	3823
	max	72	634	2.25×10^4
	STDV	0.25	4.38	192
$PM_{2.5}$ (µg/m³)	min	45	111	129
	mean	50	195	4060
	max	169	712	2.31×10^4
	STDV	0.81	4.89	201
PM_4 (µg/m³)	min	45	112	138
	mean	51	200	4896
	max	170	766	2.61×10^4
	STDV	0.80	5.04	239
PM_{10} (µg/m³)	min	45	112	182
	mean	54	213	1.00×10^4
	max	173	771	5.11×10^4
	STDV	0.87	5.18	501
PM_{total} (µg/m³)	min	45	112	363
	mean	57	230	2.08×10^4
	max	185	783	1.01×10^5

	STDV	1.41	5.61	1004	

Table 3. Descriptive statistics for DustTrak (Zone 1). Adapted from Sabanov et al. (2024)

Parameter	PM_1 (µg/m³)	$PM_{2.5}$ (µg/m³)	PM_4 (µg/m³)	PM_{10} (µg/m³)	PM Total (µg/m³)
Mean	47.87	49.55	50.67	53.49	57.46
Standard Error	0.25	0.81	0.80	0.87	1.41
Median	47	48	49	51	51
Mode	46	47	48	48	48
Standard Deviation	3.63	11.86	11.83	12.85	20.79
Sample Variance	13.18	140.78	139.90	165.09	432.34
Kurtosis	16.29	86.19	85.54	65.30	17.38
Skewness	3.62	8.97	8.91	7.39	3.95
Range	28	124	125	128	140
Minimum	44	45	45	45	45
Maximum	72	169	170	173	185
Sum	1.03×10^4	1.07×10^4	1.09×10^4	1.16×10^4	1.24×10^4
Count	216	216	216	216	216
Largest (1)	72	169	170	173	185
Smallest (1)	44	45	45	45	45

Table 4. Descriptive statistics for Partector 2 (Zone 1). Adapted from Sabanov et al. (2024)

Parameter	Surface (µm²/cm³)	Mass Concentration (µg/m³)	PNC (cm^{-3})	Diameter (nm)	LDSA (µm²/cm³)
Mean	1027.96	37.97	3.44×10^4	65.31	124.90
Standard Error	45845	0.47	413.24	0.49	0.30
Median	1053.41	39.74	3.27×10^4	67	124.80
Mode	940.91	39.38	3.50×10^4	68	122.40
Standard Deviation	104.34	6.96	6101.39	7.30	4.44
Sample Variance	1.09×10^4	48.49	3.73×10^7	53.29	19.69
Kurtosis	7.34	3.87	10.54	5.23	-0.26
Skewness	-2.39	-1.75	2.84	- 1.99	0.13
Range	689.36	41.68	4.26×10^4	45	24.20
Minimum	501.41	8.95	2.62×10^4	32	112
Maximum	1190.77	50.63	6.88×10^4	77	136.20
Sum	2.24×10^5	8278.03	7.49×10^6	1.42×10^4	2.72×10^4
Count	218	218	218	218	218
Largest (1)	1190.77	50.63	6.88×10^4	77	136.20
Smallest (1)	501.41	8.95	2.62×10^4	32	112

Table 5. Descriptive statistics for DustTrak (Zone 2). Adapted from Sabanov et al. (2024)

Parameter	PM_1 (µg/m³)	$PM_{2.5}$ (µg/m³)	PM_4 (µg/m³)	PM_{10} (µg/m³)	PM Total (µg/m³)
Mean	189.62	194.79	199.64	212.97	230.08
Standard Error	4.38	4.89	5.04	5.18	5.61
Median	147	149	153.50	173.50	200.50
Mode	123	139	142	135	147

Standard Deviation	82.58	92.28	95.13	97.72	105.93
Sample Variance	6820.07	8515.66	9048.82	9549.10	11,221.59
Kurtosis	3.60	7.36	8.21	7.60	6.38
Skewness	1.57	2.15	2.23	2.13	1.94
Range	539	601	654	659	671
Minimum	95	111	112	112	112
Maximum	634	712	766	771	783
Sum	6.75×10^4	6.93×10^4	7.11×10^4	7.58×10^4	8.19×10^4
Count	356	356	356	356	356
Largest (1)	634	712	766	771	783
Smallest (1)	95	111	112	112	112

Table 6. Descriptive statistics for Partector 2 (Zone 2). Adapted from Sabanov et al. (2024)

Parameter	**Surface ($\mu m^2/cm^3$)**	**Mass Concentration ($\mu g/m^3$)**	**PNC (cm^{-3})**	**Diameter (nm)**	**LDSA ($\mu m^2/cm^3$)**
Mean	3246.37	88.82	2.48×10^5	59.13	554.36
Standard Error	152.92	3.24	18011.34	0.84	32.60
Median	1512.57	59.99	4.87×10^4	65	173.95
Mode	891.84	20.56	4.39×10^4	65	159.60
Standard Deviation	2885.34	61.07	3.40×10^5	15.90	615.16
Sample Variance	8.33×10^6	3729.87	1.15×10^{11}	252.81	3.78×10^5
Kurtosis	-0.31	4.73	0.77	1.73	-0.37
Skewness	1.19	1.84	1.43	0.06	1.14
Range	1.34×10^4	459.94	1.34×10^6	122	2109.20
Minimum	1.42×10^4	475.41	2.26×10^4	28	141.50
Maximum	1.16×10^6	3.16×10^4	1.36×10^6	150	2250.7
Sum	356	356	8.82×10^7	2.11×10^4	1.97×10^5
Count	1.42×10^4	475.41	356	356	356
Largest (1)	743.78	15.47	1.36×10^6	150	2250.7
Smallest (1)	3246.37	88.82	2.26×10^4	28	141.5

Table 7. Descriptive statistics for DustTrak (Zone 3). Adapted from Sabanov et al. (2024)

Parameter	**PM_1 ($\mu g/m^3$)**	**$PM_{2.5}$ ($\mu g/m^3$)**	**PM_4 ($\mu g/m^3$)**	**PM_{10} ($\mu g/m^3$)**	**PM Total ($\mu g/m^3$)**
Mean	3823.06	4060.39	4895.51	1.00×10^4	2.08×10^4
Standard Error	191.97	200.82	238.89	500.87	1003.65
Median	2625	2815	3365	6665	1.47×10^4
Mode	1010	1.08×10^4	2900	1.32×104	1.17×10^4
Standard Deviation	3952.90	4135.13	4919.25	1.03×10^4	2.07×10^4
Sample Variance	1.56×10^7	1.71×10^7	2.42×10^7	1.06×10^8	4.27×10^8
Kurtosis	2.86	2.53	1.95	1.67	1.13
Skewness	1.59	1.52	1.42	1.39	1.25
Range	2.24×10^4	2.30×10^4	2.60×10^4	5.09×10^4	1.01×10^5
Minimum	124	129	138	182	363
Maximum	2.25×10^4	2.31×10^4	2.61×10^4	5.11×10^4	1.01×10^5
Sum	1.62×10^6	1.72×10^6	2.08×10^6	4.26×10^6	8.84×10^6

Count	424	424	424	424	424
Largest (1)	2.25×10^4	2.31×10^4	2.61×10^4	5.11×10^4	1.01×10^5
Smallest (1)	124	129	138	182	363

Table 8. Descriptive statistics for Partector 2 (Zone 3). Adapted from Sabanov et al. (2024)

Parameter	**Surface ($\mu m^2/cm^3$)**	**Mass Concentration ($\mu g/m^3$)**	**PNC (cm^{-3})**	**Diameter (nm)**	**LDSA ($\mu m^2/cm^3$)**
Mean	2426.99	69.58	1.39×10^5	53.71	372.12
Standard Error	72.41	1.98	5669.54	0.61	12.11
Median	1895.29	56.34	9.86×10^4	52	289.95
Mode	#N/A	55.72	5.96×10^4	46	179.10
Standard Deviation	1490.99	40.73	1.17×10^5	12.64	249.44
Sample Variance	2.22×10^6	1659.40	1.36×10^{10}	159.69	6.22×10^4
Kurtosis	10.60	14.54	13.24	20.30	7.93
Skewness	2.81	3.23	2.81	3.08	2.38
Range	1.07×10^4	343.49	1.00×10^6	120	1687.30
Minimum	1036	25	2.49×10^4	30	160.70
Maximum	1.17×10^4	368.53	1.02×10^6	150	1848
Sum	1.03×10^6	2.95×10^4	5.91×10^7	2.28×10^4	1.58×10^5
Count	424	424	424	424	424
Largest (1)	1.17×10^4	368.53	1.02×10^6	150	1848
Smallest (1)	1036.26	25.04	2.49×10^4	30	160.70

From Figure 7, Zone 2, it can be observed that the data obtained from the loader diesel engine emissions created particles with a diameter of 30–70 nm. Particle diameters over 90 nm are mostly received from the dumping peaks, and are mostly associated with oil shale dust, which consists of over 80% of carbon particles, as per the results obtained from the filter SEM/EDS analysis.

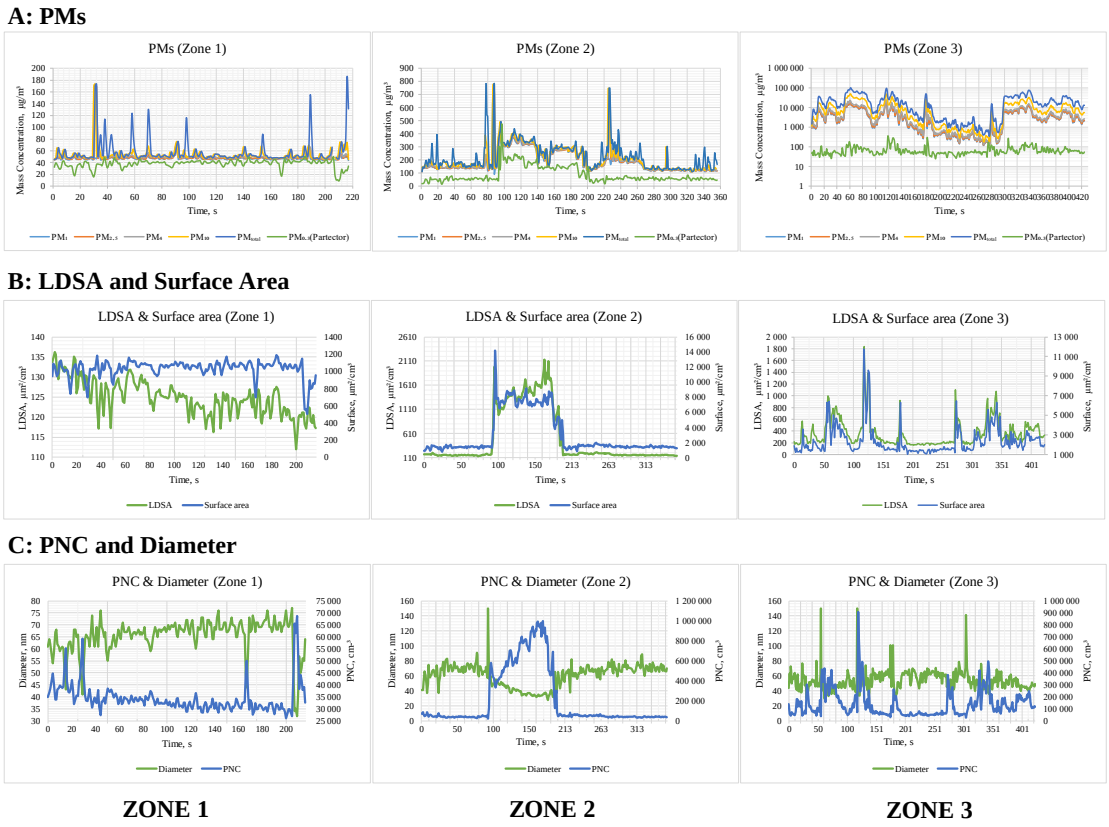

Figure 7. Results of measurements in three zones. Adapted from Sabanov et al. (2024)

4.2 Filter Analysis by SEM/EDS (Jeol JSM-IT200)

The SEM/EDS apparatus tested the mesh filter used in the DustTrak instrument. The results showed that the mesh filter contained four elements in total. The mesh filter morphology image was observed at a scale of 10 µm (Figure 8a) and showed the carbon particles. These particles are mostly clustered and irregular in symmetry. Most of the particles are spherical in shape and agglomerated. Assuming that the DPM particle size is smaller than one micrometer, most of the particles in Figure 7a can be related to oil shale dust particles. Figure 8b displays the elemental mass concentration and highlights the SEM/EDS peaks for each element, along with associated intensity counts and energy dispersive X-ray.

The SEM/EDS analysis of the filter revealed a diverse elemental composition, with four elements identified. Carbon and oxygen emerged as the predominant elements, constituting the major elemental composition. Notably, gold (Au) and copper (Cu) were also detected, albeit in traces, each contributing to less than 2% of the total mass concentration. Consequently, these two elements were excluded from further analysis due to their minimal impact on the overall

composition. This elemental distribution pattern remained consistent across various monitoring points on the sample filter.

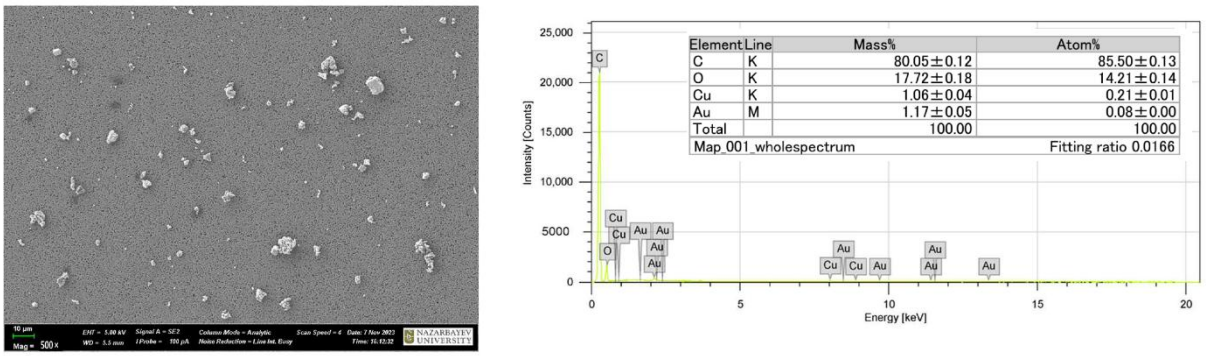

(a) (b)

Figure 8. Filter Analysis by SEM/EDS: (a) morphology; (b) elemental mass concentration. Adapted from Sabanov et al. (2024)

4.3 Data Analysis

Relationships between PM and LDSA were produced using the linear regression model with a single explanatory variable. Results for Zone 2 are presented in Figure 9, and demonstrate the best $R^2 = 0.52$ for PM_1 compared to other PMs. For this relationship in Zone 2, the data used only the diesel engine exhaust, when it worked on its nominal RPM.

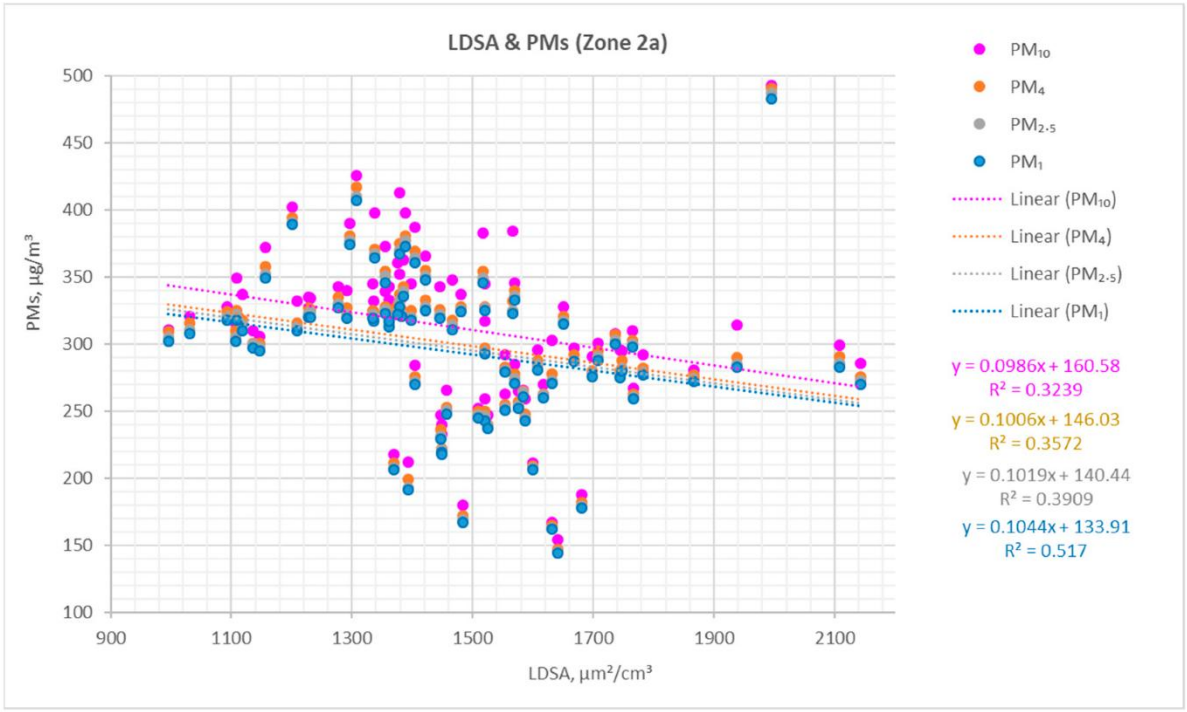

Figure 9. Linear relationships of LDSA and PM for Zone 2. Adapted from Sabanov et al. (2024)

However, from Figure 10, it can be observed that the highest $R^2 = 0.46$ is for PM_{10}, and PM_1 has $R^2 = 0.37$.

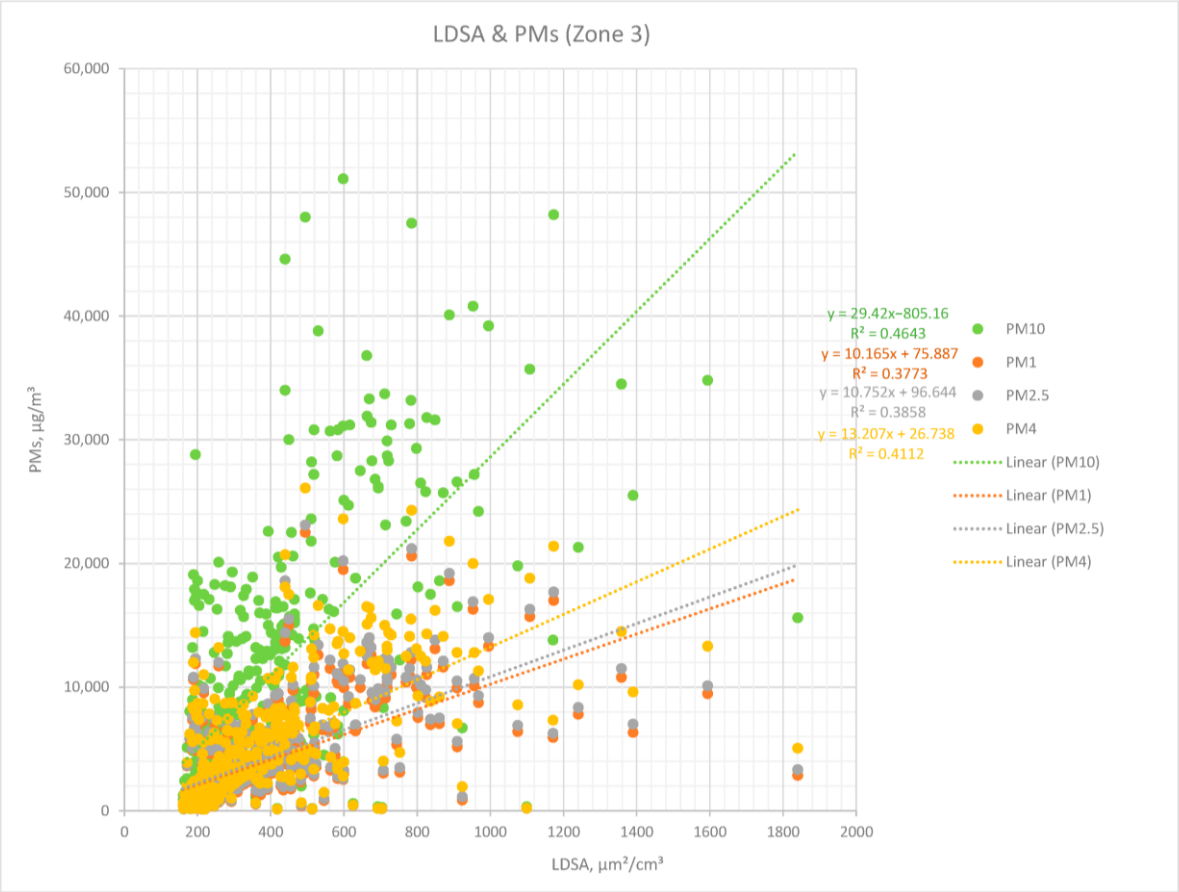

Figure 10. Linear relationships of LDSA and PM for Zone 3. Adapted from Sabanov et al. (2024)

This happened in Zone 3 due to some high peaks associated with the dumping emissions; thus, the relationship can be better presented through nonlinear trend lines. These results can be found in Figures 11 and 12. The relationships between PNC, PM_1, PM_{10}, and $PM_{0.3}$ were examined through best-fit trend lines. In Zone 1, results revealed low correlations with $R^2 = 0.0004$ for PNC and PM_1 and $R^2 = 3 \times 10^{-5}$ for PM_1 and $PM_{0.3}$. Conversely, a notable correlation, $R^2 = 0.84$ between PNC and $PM_{0.3}$ was observed. It should be noted that PNC and $PM_{0.3}$ data were received from the same instrument (Partector 2) and demonstrated its reliability for such measurements in the oil shale underground mine atmosphere. In Figure 11, Zone 2 showed better correlations for PNC and PM_1 with $R^2 = 0.57$, and for PM_1 and $PM_{0.3}$ with $R^2 = 0.55$; however, there are some deviations to $R^2 = 0.62$ for PNC and $PM_{0.3}$ compared to Zone 1. Zone 3 demonstrated correlations for PNC and PM_1 with $R^2 = 0.32$, some decreases of $R^2 = 0.12$ for PM_1 and $PM_{0.3}$, and $R^2 = 0.31$ for PNC and $PM_{0.3}$ (Figure 11).

In addition, LDSA was compared to PNC, $PM_{0.3}$, PM_1, and PM_{total} showed a good correlation in Zone 2 for LDSA/PNC with $R^2 = 0.95$, LDSA/PM_{total} with $R^2 = 0.49$, LDSA/$PM_{0.3}$ with $R^2 = 0.77$, and LDSA/PM_1 with $R^2 = 0.64$. Zone 3 LDSA/PNC has $R^2 = 0.72$, LDSA/PM_{total} has $R^2 = 0.49$, and LDSA/$PM_{0.3}$ has $R^2 = 0.55$. LDSA/PM_1 has $R^2 = 0.45$ (Figure 12).

Considering that in Zone 2, measurements were mostly related to DPM, and the Partector instrument was more sensitive for sampling fine particles, the PNC and LDSA demonstrated the best relationships. In Zone 3, dumping created dust particles, thus the LDSA/PM_{total} has a better correlation than in Zone 2.

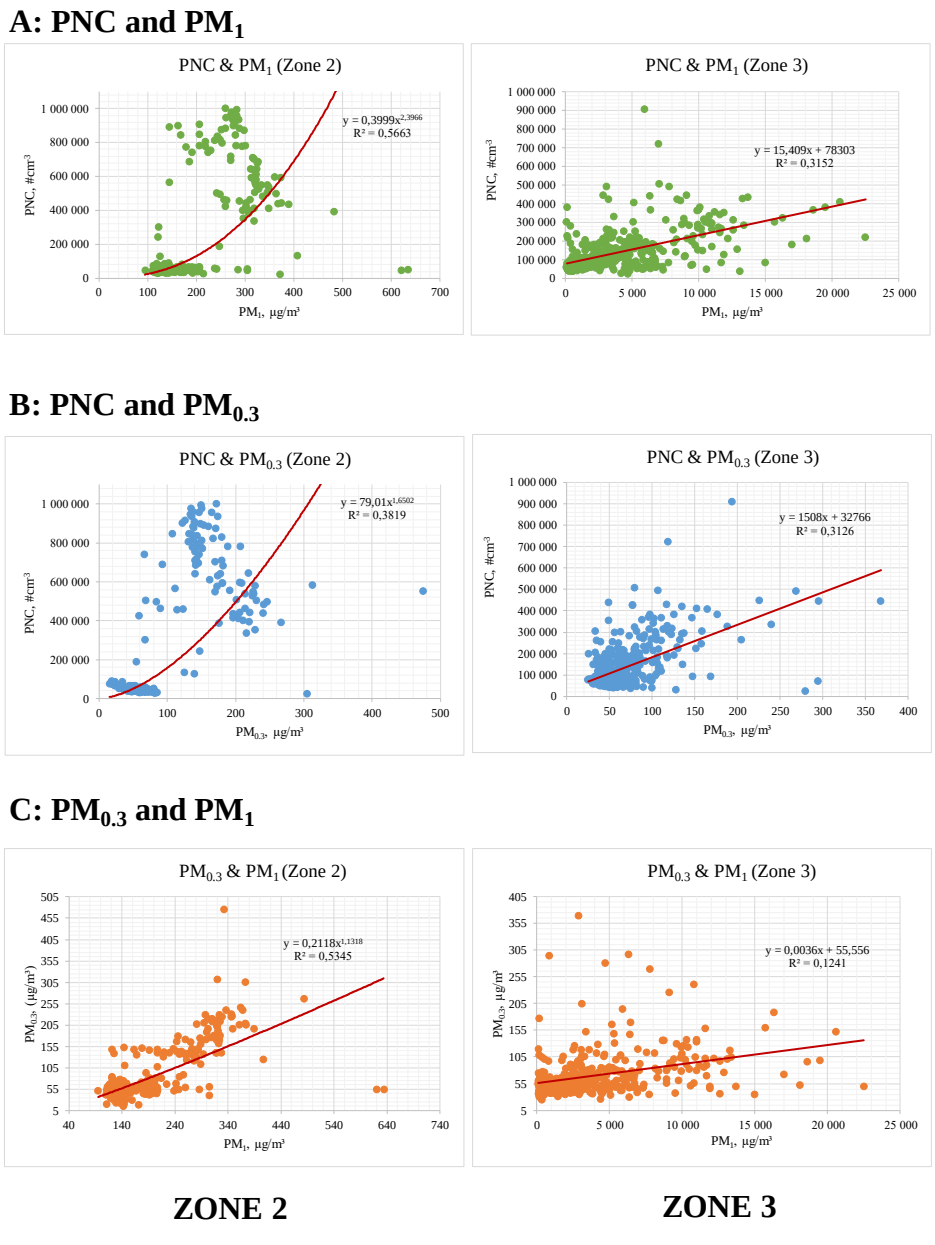

Figure 11. Relationships between PNC, PM_1, and $PM_{0.3}$ in Zone 2 and Zone 3. Adapted from Sabanov et al. (2024)

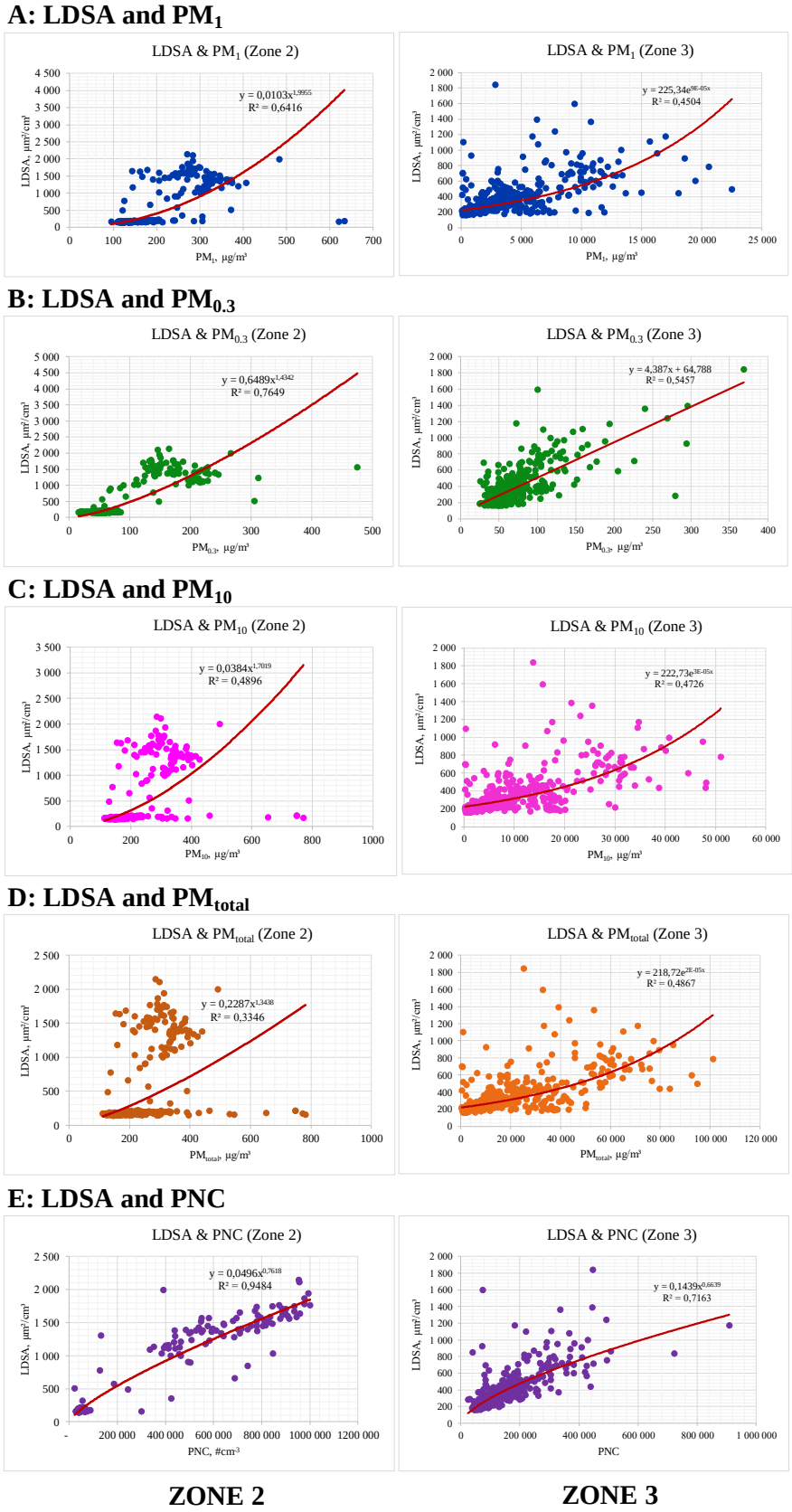

Figure 12. Relationships between LDSA, PNC, PM_1, PM_{10}, $PM_{0.3}$, and PM_{total} in Zone 2 and Zone 3. Adapted from Sabanov et al. (2024)

4.4 Particle Diameter Analysis

The time-series trends of the PM concentration in Zone 3 demonstrated spikes considerably higher than the baseline PM concentration in Zone 2, which measured diesel exhaust gases related to DPM emissions. Particle diameter ranged from 30 to 90 nm (Zone 2), while during the dumping peaks it varied from 90 to 160 nm (Zone 3). Figure 13 provides particle number concentration at particle diameter distributions measured at Zone 2 and Zone 3. Colored areas show different locations (Zone 1 and Zone 2) and estimated sources of emission (purple—DPM, orange—oil shale dust particles).

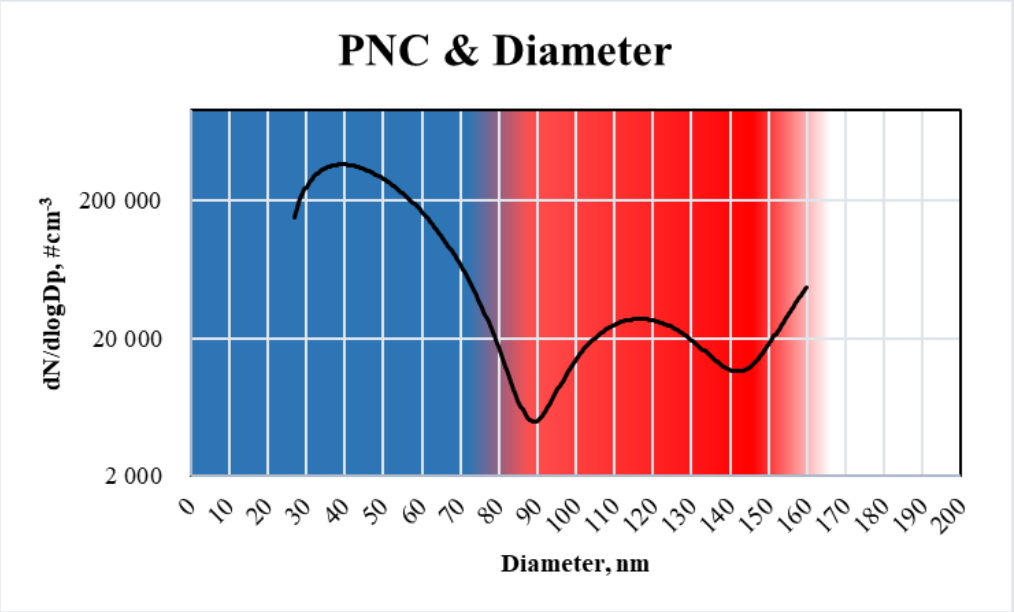

Figure 13. Particle number concentration and particle diameter distributions (blue—DPM from Zone 2, red—carbon particles from oil shale from Zone 3). Adapted from Sabanov et al. (2024)

Figure 14 demonstrates results obtained from the Monte Carlo simulation to show possible outcomes of particle diameters 34–70 nm for DPM and 92–142 nm for oil shale particulates.

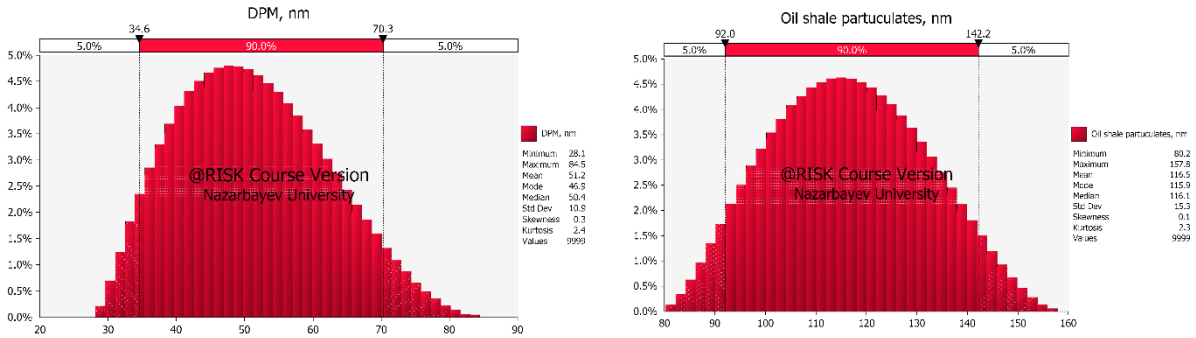

Figure 14. Variations of particle diameter for DPM and oil shale. Adapted from Sabanov et al. (2024)

For Monte Carlo simulation of LDSA and PM_1 value distribution by considering the instrument's accuracy propagation as a main variability, a PERT distribution for min, max, and weighted average values was utilised. Fit comparisons with the Weibull distribution were produced. LDSA outcomes for Zone 2 are presented in Figure 15, where values are estimated in a range of 1154–1700 $\mu m^2/cm^3$, and PM_1 in Figure 16 in a range of 198–408 $\mu g/m^3$. For Zone 3, LDSA estimated in a range of 440–1097 $\mu m^2/cm^3$ (Figure 17), and PM_1 in a range of 7147–17,142 $\mu g/m^3$ (Figure 18).

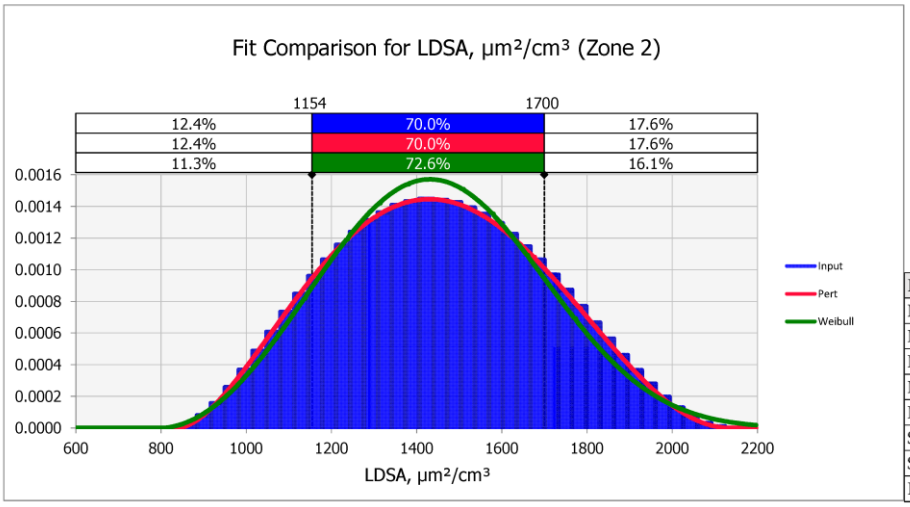

Name	Pert	Weibull
Minimum	841.1	801.0
Maximum	2142.9	+∞
Mean	1452.9	1453.5
Mode	1433.3	1434.9
Median	1448.3	1446.3
Std. Deviation	245.6	242.8
Skewness	0.1	0.2
Kurtosis	2.3	2.7

Figure 15. Fit comparison of LDSA in Zone 2. Adapted from Sabanov et al. (2024)

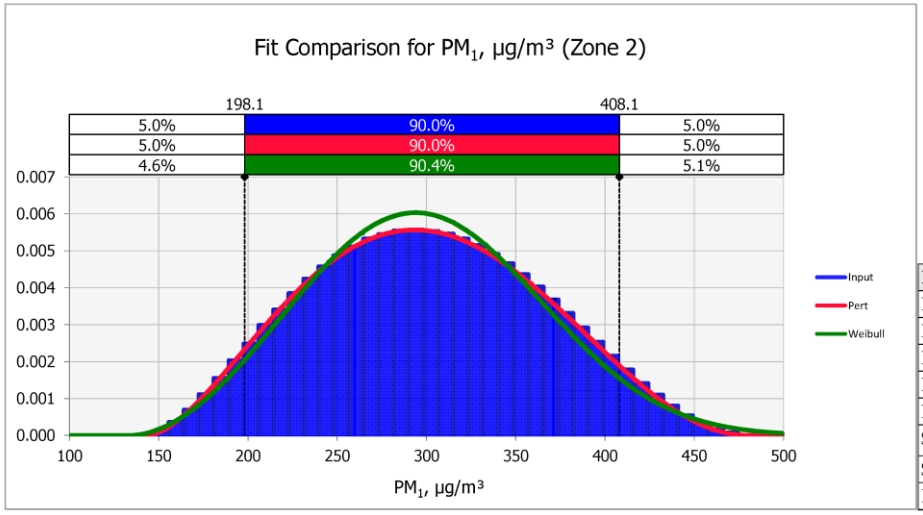

Name	Pert	Weibull
Minimum	144.0	134.7
Maximum	482.9	+∞
Mean	300.5	300.7
Mode	294.1	294.7
Median	299.0	298.5
Std. Deviation	63.9	63.2
Skewness	0.1	0.2
Kurtosis	2.3	2.8

Figure 16. Fit comparison of PM_1 in Zone 2. Adapted from Sabanov et al. (2024)

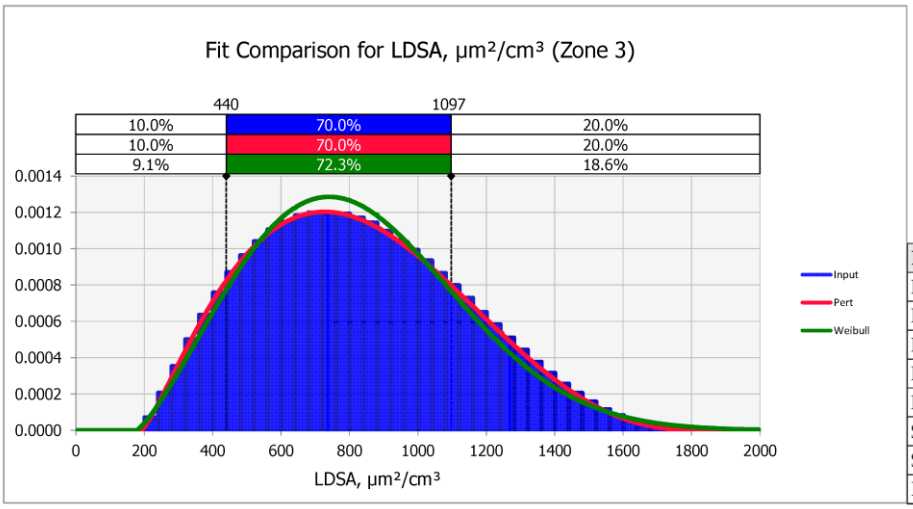

Name	Pert	Weibull
Minimum	194.5	181.5
Maximum	1839.4	+∞
Mean	826.1	826.3
Mode	730.7	744.4
Median	803.7	800.7
Std. Deviation	302.4	301.4
Skewness	0.3	0.5
Kurtosis	2.5	3.0

Figure 17. Fit comparison of LDSA in Zone 3. Adapted from Sabanov et al. (2024)

Zone 2 is characterized by more stable data and is therefore pretty close to a normal distribution. A probability bin limit of 0.001 was chosen to fit the Partector 2 instrument accuracy interval to obtain at least 70% confidence. For DustTrak, a 90% confidence level has been used. Zone 3 has spikes associated with dumping operations, and therefore, values have higher deviations. For Zone 3, a probability bin limit of 0.0008 was chosen for LDSA (Figure 18).

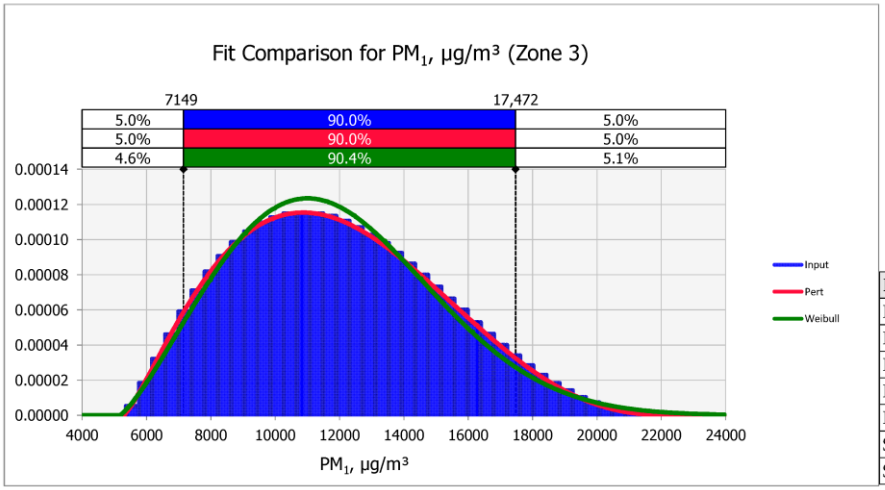

Name	Pert	Weibull
Minimum	5319.5	5202.7
Maximum	22,465.8	+∞
Mean	11,903.9	11,903.9
Mode	10,909.5	11,042.5
Median	11,669.9	11,635.0
Std. Deviation	3152.0	3140.6
Skewness	0.3	0.5

Figure 18. Fit comparison of PM_1 in Zone 3. Adapted from Sabanov et al. (2024)

4.5 Ventsim Simulation Results

Figures 19 and 20 show how DPM generated by diesel equipment in an underground oil shale mine is distributed over time. Initially, after 30 minutes, the concentration of contamination is high in the immediate vicinity of the source. As time increases (1-6 hours), the pollutants spread further, covering a larger area of the mine. The ventilation system plays a key role in controlling

the spread of pollution by directing the flow of air and reducing concentrations in certain areas. However, despite ventilation, there is an overall increase in the area of contamination over time, which highlights the need for effective measures to control and reduce diesel particle emissions in the mine to ensure the safety of workers.

Figure 21 demonstrates 6 graphs (corresponding to six numbered monitoring markers) showing the change in the concentration of DPM over time at each point. The shapes of the graphs vary, suggesting different behaviors of DPM concentration at various parts of the mine. Graphs 1 and 3 indicate a stable concentration, while graphs 2, 4 and 5 show sharp variations, and graph 6 shows a gradual increase in concentration. Based on the graphs, for points 1 and 3, the monitors regularly show low DPM concentrations. This could imply that these regions are either remote from the emission source (1) or have effective ventilation (3). For points 2, 4, and 5, the monitors show a consistent but relatively high DPM concentration, with a surge in values at the start of the measurements suggesting proximity to the pollution source and a concentration that declines slightly with time but remains stable. The final point, 6, demonstrates a gradual increase in DPM over time. This could suggest a spot in an area where particles accumulate owing to limited ventilation.

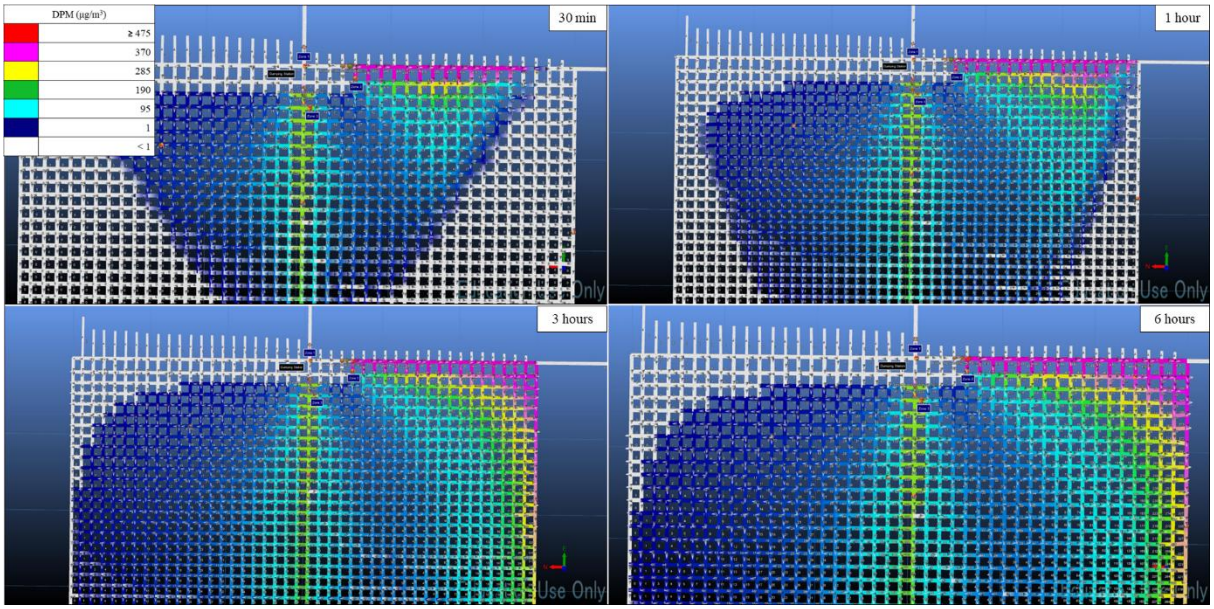

Figure 19. Dynamics of DPM (µg/m^3) distribution in Ventsim

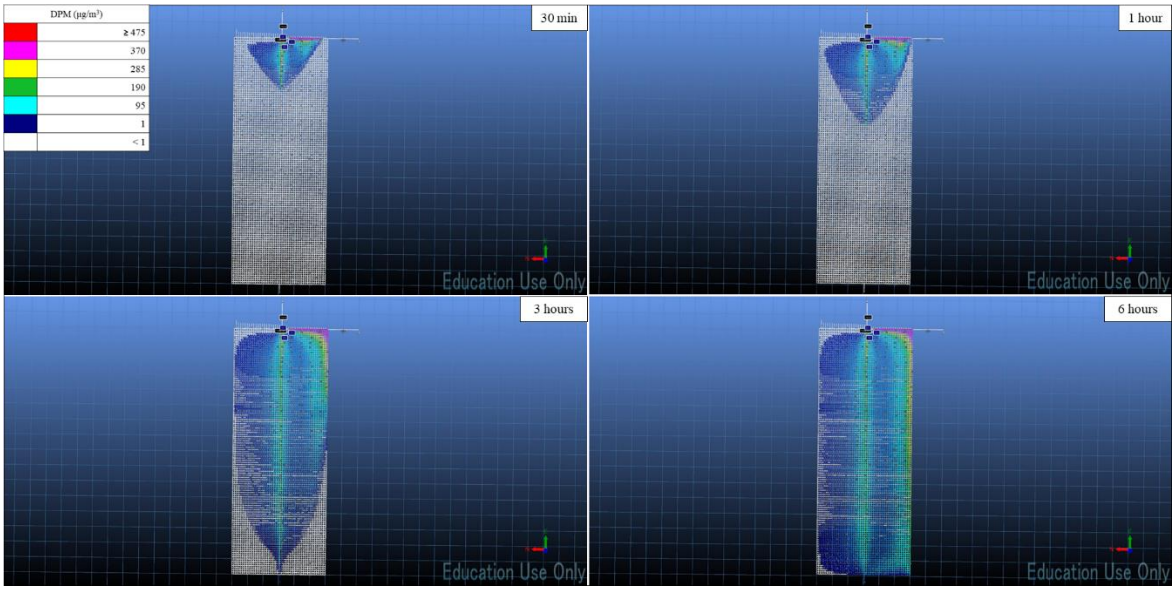

Figure 20. Dynamics of DPM (µg/m^3) distribution in Ventsim (full view)

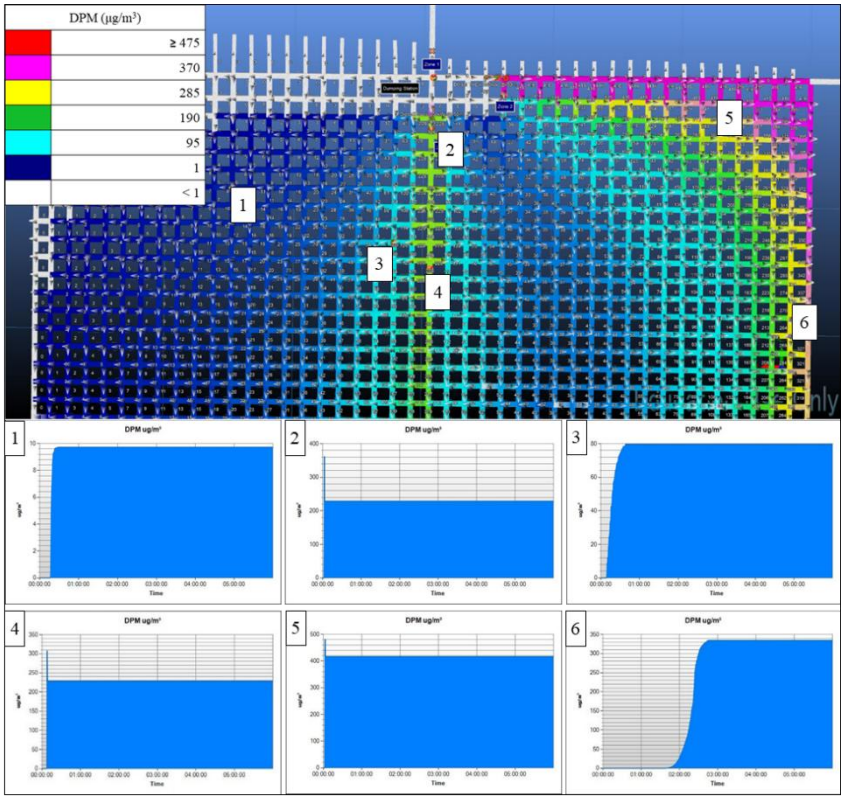

Figure 21. Analysis of DPM (µg/m^3) distribution in Ventsim using dynamic monitors

Figures 22 and 23 illustrate the dynamics of dust distribution in the mine: initially, the particles accumulate at the source, then disperse rapidly across the working area, reaching remote areas within 3 hours, and progressively dissipating by 6 hours. The findings underscore the need for efficient ventilation for miner safety and to enhance the ventilation system. Similar to the previous case, Figure 24 shows graphs showing changes in the dust concentration for each point selected for monitoring. For point 1, the monitors show a sharp concentration spike about 20

minutes after the start of the simulation, followed by a plateau with relatively low dust concentrations. This indicates that the monitor is located at a short distance from the emission source, and the particles quickly reach it. For points 2, 3 and 4, the graphs show a sharp increase in concentration at the beginning, then stabilization at a high level. This indicates that these points are located close to both sources of dust emissions or in an area where polluted air is rapidly entering. The graphs for points 5 and 6 most likely show a delayed and gradual increase in concentration, which indicates that the monitor is located in an area with very weak airflow, where particles spread slowly, or that particles reached the sensor with a delay, but in high concentration.

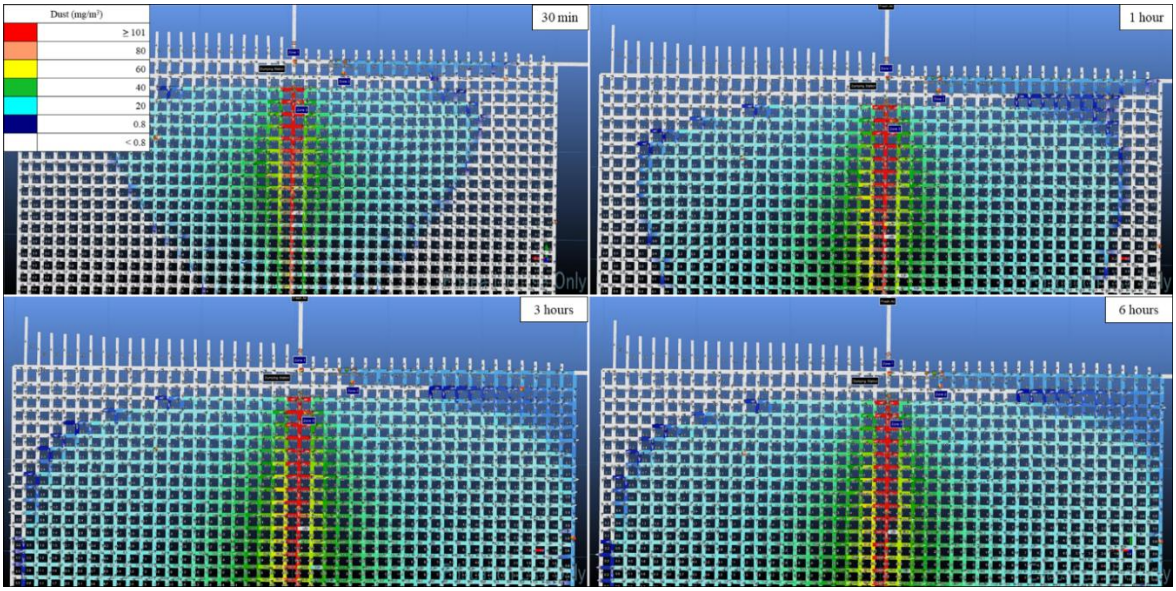

Figure 22. Dynamics of dust (mg/m^3) distribution in Ventsim

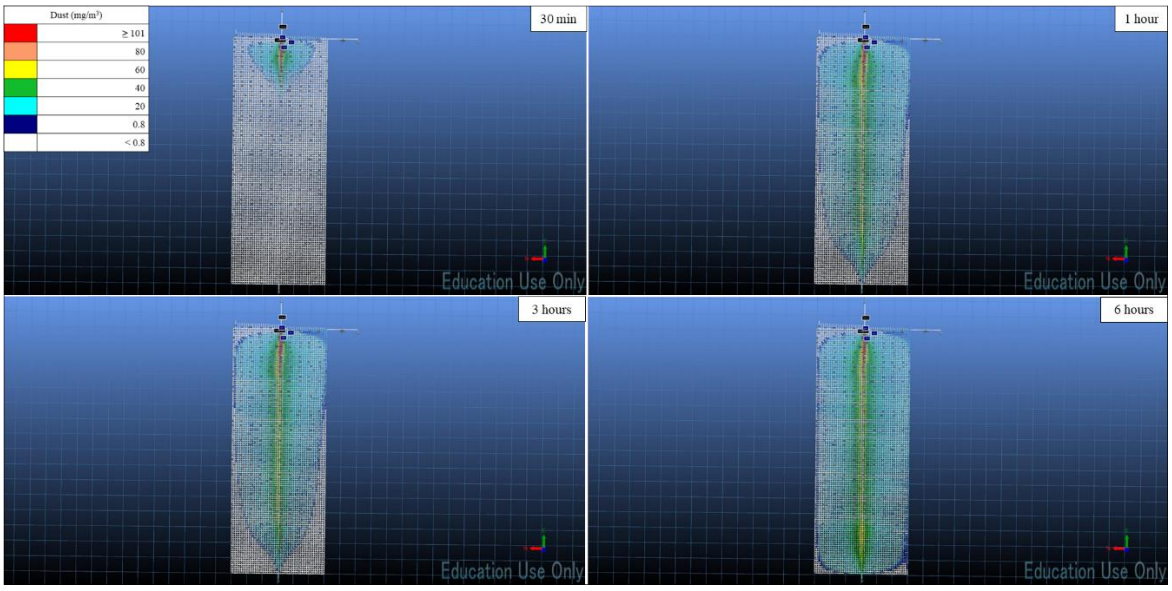

Figure 23. Dynamics of dust (mg/m^3) distribution in Ventsim (full view)

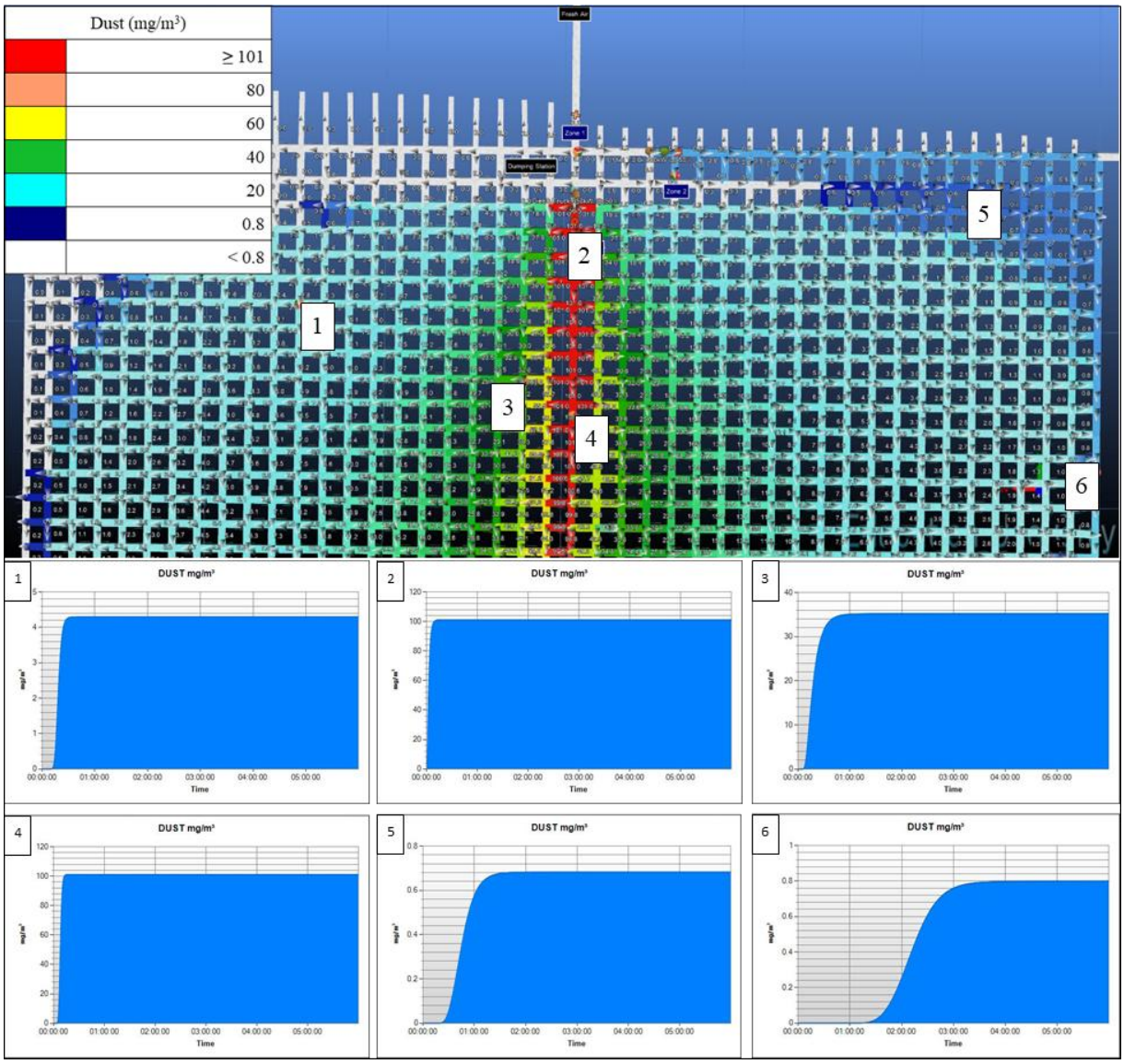

Figure 24. Analysis of dust (mg/m^3) distribution in Ventsim using dynamic monitors

Thus, the simulation offered a visual and quantitative representation of DPM and dust distribution, emphasizing areas of high concentration and possible accumulation. The Ventsim results validated the experimental data, indicating that areas directly impacted by loading and dumping processes displayed the highest concentrations. The simulation demonstrated the impact of ventilation patterns on the distribution of these contaminants, identifying possible directions for their spread to other work locations.

5. DISCUSSION

5.1 Compliance of the Results Obtained with the Research Hypothesis

The relationship between PM and LDSA concentrations measured by two different instruments does not have a great R^2 factor, and it might not be recommended to use one instrument separately for measurements. Partector 2 demonstrated its reliability to be used for measurements of gaseous aerosols, i.e., DPM, and DustTrak is more suitable for solid particles, i.e., oil shale dust particulates. This can be applied to coal particulates as well. By these experimental measurements, particle diameter distributions in relation to PNC have been produced, and showed that a particle diameter of 30–90 nm is related to DPM, and a diameter of 90 to 160 nm is associated with oil shale dust particulates.

Because the diffusion charger utilised by Partector 2 is not a reference method to calculate PNC, the Condensation Particle Counter (CPC) model 3007, TSI, USA, was used as a reference monitor for collation measurements to obtain a calibration factor (Jafarigol et al., 2023). The diffusion charging method showed a reasonable correlation with the reference CPC if solid particles exist. However, the weakest part of this method is the assumption that solid and volatile particles are in agglomeration mode. To prove this, the particle size distribution will be required (Jafarigol et al., 2023).

Braakhuis et al. (2014), Kuuluvainen et al. (2016), Kuula et al. (2020), Tran et al. (2020), Afshar-Mohajer et al. (2020), and Huynh et al. (2018) derived that diesel particulates occur in two size modes, where <1.0 μm single particles are dominant, and about 10% are >1.0 μm due to agglomeration. Therefore, it is difficult to determine the total amount present if mixed with coal, as it is combustible carbon-based. Thus, based on the above-mentioned research studies' outcomes, 0.8 μm can provide an approximate split between DPM and carbon dust. According to our measurements, the split is close to 0.01 μm, which is relevant for the nuclei mode of diesel engine exhaust gases. To confirm these hypotheses, the elemental or total carbon filter measurements need to be produced, and mass size distributions should be calculated.

LDSA in Zone 2 during the high RPM of the diesel loader engine (DPM stage) reached an average concentration of 1455 $\mu m^2/cm^3$, and in Zone 3 within the dumping peaks, it reached an average concentration of about 830 $\mu m^2/cm^3$. However, in Zone 3, excluding the dumping peaks, the averaged LDSA was around 370 $\mu m^2/cm^3$. Compared to other studies of LDSA values, this study's results highlight the high emissions associated with DPM at high diesel

engine RPM during the loading process, and the high dump peaks (oil shale dust) in the dumping process.

5.2 Limitation of this Study and Generalization of Its Results

This investigation was restricted to the quantification of black carbon, elemental or total carbon, particle size distribution, and time duration; therefore, it is not feasible to apply these results to establish standard exposure limits. Gaining insight into particulate matter morphology is valuable due to its direct correlation with elemental composition (Panda & Nagendra, 2018). The morphology of particles, which significantly affects toxicity due to the increase in the sorption potential of dust particles with increasing surface area, has not been discussed in this study, due to limited experimental measurements. The toxicity of dust particles depends on their origin, shape, reactivity, surface chemistry, and charge. If the shape of a particle changes, affecting the diffusion speed, then the hydrodynamic size will also change. Anthropogenic particles are characterized by more spherical shapes due to combustion processes (Puławska et al., 2021; Sarver et al., 2019; Trechera et al., 2020; Schriefl et al., 2020; Chen et al., 2023). Particle size and shape of samples could result from the presence of different mineralogical phases (Schiavo et al., 2023). Many researchers have stated that particle shape may have great impact on its toxicity (Puławska et al., 2021; Sarver et al., 2019; Trechera et al., 2020; Schriefl et al., 2020; Chen et al., 2023). Filter sampling duration was produced in a short time interval, and therefore did not show the entire chemical composition. This could be one of the primary reasons for the chemical composition's homogeneity in carbon and oxygen elements. Particle size distribution analysis by selecting representative images from SEM should be performed. Proper sampling of DPM will require PTFE filters (25 mm or 37 mm) to collect elemental composition, and quartz filters (37 mm) to collect carbonaceous components.

The complexity of determining UFPs could result in greater errors in measurements. The unknown shape of the particle size distribution plays a significant role in determining the measurement uncertainty of Partector 2. It is calibrated for lognormal particle size distributions with a geometric standard deviation of 1.9, which is a reasonable assumption for many environments. In the case of measurements of particles of only a specific diameter (monodisperse particles), the Partector 2 diameter determination will be inaccurate, as will the number, surface, and mass determination.

The accuracy and precision of the measured and corrected DustTrak measurements were not evaluated against the reference measurements due to the absence of gravimetric analysis. Thus,

correction factors need to be determined and applied to the results. Li et al. (2019) reported correction factors (0.31–0.43) for DustTrak 30-min $PM_{2.5}$ at RH conditions (50–90%). DustTrak underestimated PM_{10} mass concentrations (24 h average) by about 20% compared to the reference gravimetric method. DustTrak PM_{10} measurements have better accuracy (19.83%) but lower precision (R^2 = 0.73) than $PM_{2.5}$ measurements. Particularly, the gravimetric method's measurement of DustTrak PM_{10} readings at higher PM10 levels (>200 g m−3) reveals relatively low precision (Javed & Guo, 2021).

5.3 Proposals for Practical Application

LDSA, as a rather new metric, is still rarely included in long-term air quality monitoring networks. LDSA can be alternatively calculated by lung deposition models and particle size distributions (Kuula et al., 2020; Fung et al., 2022), however, measurements of the full spectrum of particle size distributions are not common either. Increased peak concentrations during the dumping process and personal exposure to toxic aerosols are, therefore, miners' health concerns. Based on the study outcomes, it is proposed to use direct-reading aerosol instruments to monitor real-time exposures to miners and for air quality control. A better design and planning of auxiliary ventilation and the relocation of miners cleaning the conveyor belt away from the dumping point may reduce personal exposure to freshly emitted airborne particles. Carrying out a working shift assessment of LDSA exposure to miners by recording individual time–activity exercises can be recommended. Such a universally applicable personal exposure assessment will help with mine site measurements in the context of a miner's health risk assessment and miners' well-being improvement. Electric loaders can be proposed to be used to improve mine air quality with miners' health benefits. Global ramifications for occupational safety regulations and public health policies can result from a more detailed study of LDSA in terms of cross-industry applications.

5.4 Mitigation of PM-Related Health Risks in Mining Environments

PM is a major health and safety hazard in underground mining sites because it can induce respiratory and cardiovascular ailments in miners. Fine particles produced by drilling, blasting, diesel equipment, and material handling can build up in tight spaces, causing long-term occupational risks. To reduce the risk presented by PM in underground mines, a multifaceted approach combining engineering controls, administrative measures, and personal protective techniques is required. First and foremost, adequate ventilation systems should be constructed

and maintained on a regular basis to dilute and remove airborne particulates from working environments. The adoption of low-emission diesel engines and diesel particulate filters (DPFs) can greatly reduce fine particle emissions. Regular maintenance of mining equipment also contributes to reduced emissions. Furthermore, water spraying and dust suppression systems at drilling, blasting, and loading points are useful in reducing dust at its source. Administrative controls, such as scheduling labour to reduce miners' time in high-exposure zones and rotating duties, can help to restrict individual exposure. Finally, regular use of proper personal protective equipment (PPE), such as high-efficiency respirators, adds another layer of protection, particularly in regions where engineering and administrative controls are insufficient. Monitoring mechanisms should be in place to regularly measure PM concentrations and ensure adherence to occupational exposure guidelines.

5.5 Suggestion for Future Research Direction

Future studies on particle matter in oil shale mines can be focused on exposure time, particle nuclei mode and agglomeration mode, and long-term impact estimation on the human body. Exposure limits should be elaborated and represented for nanoparticles, and therefore LDSA can be an option to use as a measure to demonstrate health relevance. Work out methodologies to represent LDSA as an indicator for air quality monitoring in relation to nanoparticles, and recommend setting up exposure standards for miners.

6. CONCLUSIONS AND RECOMMENDATIONS

During the study, the analysis was conducted on PMs, LDSA, average particle diameter and PNC producing a few valuable correlation factors. Analyses of PM and LDSA concentrations in the operational areas of the oil shale underground mine revealed that PM and LDSA levels fluctuated significantly during loading and unloading, as validated by simulation results. Averaged LDSA was around 1433 $\mu m^2/cm^3$ and reached maximum peaks of 2140 $\mu m^2/cm^3$ during the loading, which was mostly related to diesel exhaust emissions, and within the dumping, 730 $\mu m^2/cm^3$ and 1840 $\mu m^2/cm^3$, respectively. At the same time, average PM_1 was about 300 $\mu g/ m^3$ during the loading, but within the dumping peaks, it reached up to 10,900 $\mu g/m^3$. During the loading phase, particle diameter ranged from 30 to 90 nm, while during the dumping phase peaks, it varied from 90 to 160 nm. Variations of particle diameter for DPM and oil shale, and LDSA and PM_1 values distribution for consideration of the instrument's accuracy variability have been run with the help of a Monte Carlo simulation to demonstrate possible outcomes using a PERT distribution. A relationship between PNC and particle diameter distribution was produced, and demonstrated an approximate split between DPM and oil shale dust. The Ventsim simulation demonstrated a potential concentration of diesel and dust particles in a remote area of the mine where no direct measurements had been conducted. This study offers important data on PM and LDSA concentrations that can be used to estimate potential exposure to miners at various working operations in the oil shale underground mines, and will be used for air quality control in accordance with establishing toxic aerosol health effects. Exposure limits to nanoparticles and LDSA can be an option to use as a measure to demonstrate health relevance.

7. REFERENCES

Afshar-Mohajer, N., Foos, R., Volckens, J., & Ramachandran, G. (2020). Variability of aerosol mass and number concentrations during taconite mining operations. *Journal of occupational and environmental hygiene*, *17*(1), 1-14. https://doi.org/10.1080/15459624.2019.1688823

Akinyemi, S. A., Oliveira, M. L., Nyakuma, B. B., & Dotto, G. L. (2022). Geochemical and morphological evaluations of organic and mineral aerosols in coal mining areas: A case study of Santa Catarina, Brazil. *Sustainability*, *14*(7), 3847. https://doi.org/10.3390/su14073847

Asif, Z., Chen, Z., & Han, Y. (2018). Air quality modeling for effective environmental management in the mining region. *Journal of the Air & Waste Management Association*, *68*(9), 1001-1014. https://doi.org/10.1080/10962247.2018.1463301

Azam, S., Liu, S., Bhattacharyya, S., & Mishra, D. P. (2024). Prevalence of nano-sized coal mine dust in North and Central Appalachian coal mines–Insights from SEM-EDS imaging. *Journal of Hazardous Materials*, *476*, 135226. https://doi.org/10.1016/j.jhazmat.2024.135226

Balasurya, S., Syed, A., Thomas, A. M., Marraiki, N., Elgorban, A. M., Raju, L. L., ... & Khan, S. S. (2020). Rapid colorimetric detection of mercury using silver nanoparticles in the presence of methionine. *Spectrochimica Acta Part A: Molecular and Biomolecular Spectroscopy*, *228*, 117712. https://doi.org/10.1016/j.saa.2019.117712

Barrett, C., Sarver, E., Cauda, E., Noll, J., Vanderslice, S., & Volkwein, J. (2019). Comparison of several DPM field monitors for use in underground mining applications. *Aerosol and Air Quality Research*, *19*(11), 2367-2380. https://doi.org/10.4209/aaqr.2019.06.0319

Birch, M. E., & Noll, J. D. (2004). Submicrometer elemental carbon as a selective measure of diesel particulate matter in coal mines. *Journal of Environmental Monitoring*, *6*(10), 799-806. https://doi.org/10.1039/B407507B

Bond, T. C., Doherty, S. J., Fahey, D. W., Forster, P. M., Berntsen, T., DeAngelo, B. J., ... & Zender, C. S. (2013). Bounding the role of black carbon in the climate system: A scientific assessment. *Journal of geophysical research: Atmospheres*, *118*(11), 5380-5552. https://doi.org/10.1002/jgrd.50171

Braakhuis, H. M., Park, M. V., Gosens, I., De Jong, W. H., & Cassee, F. R. (2014). Physicochemical characteristics of nanomaterials that affect pulmonary inflammation. *Particle and fibre toxicology*, *11*, 1-25. https://doi.org/10.1186/1743-8977-11-18

Burtscher, H., Künzel, S., & Hüglin, C. (1998). Characterization of particles in combustion engine exhaust. *Journal of Aerosol Science*, *29*(4), 389-396. https://doi.org/10.1016/S0021-8502(97)10001-5

Chang, P., & Xu, G. (2017). A review of the health effects and exposure-responsible relationship of diesel particulate matter for underground mines. *International Journal of Mining Science and Technology*, *27*(5), 831-838. https://doi.org/10.1016/j.ijmst.2017.07.020

Chen, D., Nie, W., Cai, P., & Liu, Z. (2018). The diffusion of dust in a fully-mechanized mining face with a mining height of 7 m and the application of wet dust-collecting nets. *Journal of Cleaner Production*, *205*, 463-476. https://doi.org/10.1016/j.jclepro.2018.09.009

Chen, Y. H., Nguyen, D., Brindley, S., Ma, T., Xia, T., Brune, J., ... & Tsai, C. S. J. (2023). The dependence of particle size on cell toxicity for modern mining dust. *Scientific Reports*, *13*(1), 5101. https://doi.org/10.1038/s41598-023-31215-5

Clark, C. E. (1962). The PERT model for the distribution of an activity time. *Operations Research*, *10*(3). https://doi.org/10.1287/opre.10.3.405

Clarke, A. D., Shinozuka, Y., Kapustin, V. N., Howell, S., Huebert, B., Doherty, S., ... & Weber, R. (2004). Size distributions and mixtures of dust and black carbon aerosol in Asian outflow: Physiochemistry and optical properties. *Journal of Geophysical Research: Atmospheres*, *109*(D15). https://doi.org/10.1029/2003JD004378

Delfino, R. J., Sioutas, C., & Malik, S. (2005). Potential role of ultrafine particles in associations between airborne particle mass and cardiovascular health. *Environmental health perspectives*, *113*(8), 934-946. https://doi.org/10.1289/ehp.7938

Di Benedetto, A., Russo, P., Amyotte, P., & Marchand, N. (2010). Modelling the effect of particle size on dust explosions. *Chemical Engineering Science*, *65*(2), 772-779. https://doi.org/10.1016/j.ces.2009.09.029

Du, C., Wang, J., & Wang, Y. (2022). Study on environmental pollution caused by dumping operation in open pit mine under different factors. *Journal of Wind Engineering and Industrial Aerodynamics*, *226*, 105044. https://doi.org/10.1016/j.jweia.2022.105044

Du, X., Fang, H., Liu, K., Xue, B., & Cai, X. (2020). Environmental evaluation of coal mines based on generalized linear model and nonlinear fuzzy analytic hierarchy. *Geofluids*, *2020*, 1-10. https://doi.org/10.1155/2020/8836908

Duan, M., Wang, Y., Ren, X., Qu, X., Cao, Y., Yang, Y., & Nian, L. (2017). Correlation analysis of three influencing factors and the dust production rate for a free-falling particle stream. *Particuology*, *34*, 126-133. https://doi.org/10.1016/j.partic.2017.03.003

Dutta, P., Mahatha, S., & De, P. (2004). A methodology for cumulative impact assessment of opencast mining projects with special reference to air quality assessment. *Impact Assessment and Project Appraisal*, *22*(3), 235-250. https://doi.org/10.3152/147154604781765905

Fatima, S., Mishra, S. K., Kumar, U., Ahlawat, A., Dabodiya, T. S., & Khosla, D. (2023). Role of morphology and chemical composition of PM for particle deposition in human respiratory system: A case study over megacity-Delhi. *Urban Climate*, *47*, 101344. https://doi.org/10.1016/j.uclim.2022.101344

Fierz, M., Meier, D., Steigmeier, P., & Burtscher, H. (2014). Aerosol measurement by induced currents. *Aerosol Science and Technology*, *48*(4), 350-357. https://doi.org/10.1080/02786826.2013.875981

Fruin, S. A., Winer, A. M., & Rodes, C. E. (2004). Black carbon concentrations in California vehicles and estimation of in-vehicle diesel exhaust particulate matter exposures.

Atmospheric Environment, *38*(25), 4123-4133. https://doi.org/10.1016/j.atmosenv.2004.04.026

Fruin, S. A., Winer, A. M., & Rodes, C. E. (2004). Black carbon concentrations in California vehicles and estimation of in-vehicle diesel exhaust particulate matter exposures. *Atmospheric Environment*, *38*(25), 4123-4133. https://doi.org/10.1016/j.atmosenv.2004.04.026

Fung, P. L., Sillanpää, S., Niemi, J. V., Kousa, A., Timonen, H., Zaidan, M. A., ... & Hussein, T. (2022). Improving the current air quality index with new particulate indicators using a robust statistical approach. *Science of the Total Environment*, *844*, 157099. https://doi.org/10.1016/j.scitotenv.2022.157099

Fung, P. L., Zaidan, M. A., Niemi, J. V., Saukko, E., Timonen, H., Kousa, A., ... & Hussein, T. (2022). Input-adaptive linear mixed-effects model for estimating alveolar lung-deposited surface area (LDSA) using multipollutant datasets. *Atmospheric Chemistry and Physics*, *22*(3), 1861-1882. https://doi.org/10.5194/acp-22-1861-2022

Galoie, M., Motamedi, A., Fan, J., & Moudi, M. (2023). Prediction of water quality under the impacts of fine dust and sand storm events using an experimental model and multivariate regression analysis. *Environmental Pollution*, *336*, 122462. https://doi.org/10.1016/j.envpol.2023.122462

Ghose, M. K. (2007). Generation and quantification of hazardous dusts from coal mining in the Indian context. *Environmental monitoring and assessment*, *130*, 35-45. https://doi.org/10.1007/s10661-006-9451-y

Gratt, L. B. (1985). Risk analysis of hazardous materials in oil shale. *Journal of hazardous materials*, *10*(2-3), 317-350. https://doi.org/10.1016/0304-3894(85)87010-2

Huynh, T., Ramachandran, G., Quick, H., Hwang, J., Raynor, P. C., Alexander, B. H., & Mandel, J. H. (2019). Ambient fine aerosol concentrations in multiple metrics in taconite mining operations. *Annals of work exposures and health*, *63*(1), 77-90. https://doi.org/10.1093/annweh/wxy086

Igogo, T., Awuah-Offei, K., Newman, A., Lowder, T., & Engel-Cox, J. (2021). Integrating renewable energy into mining operations: Opportunities, challenges, and enabling approaches. *Applied Energy*, *300*, 117375. https://doi.org/10.1016/j.apenergy.2021.117375

Jafarigol, F., Sabanov, S., Magauiya, N., Dauitbay, Z., Qureshi, A. R., Adotey, E., ... & Torkmahalleh, M. A. (2023). Particle number, mass, and surface area concentrations inside an underground metalliferous mine in Kazakhstan. *Atmospheric Pollution Research*, *14*(9), 101871. https://doi.org/10.1016/j.apr.2023.101871

Javed, W., & Guo, B. (2021). Performance evaluation of real-time DustTrak monitors for outdoor particulate mass measurements in a desert environment. *Aerosol and Air Quality Research*, *21*(6), 200631. https://doi.org/10.4209/aaqr.200631

Jeong, J., Bae, S. Y., & Choi, J. (2021). Identification of toxicity pathway of diesel particulate matter using AOP of PPARγ inactivation leading to pulmonary fibrosis. *Environment International*, *147*, 106339. https://doi.org/10.1016/j.envint.2020.106339

Jin, H., Li, S., Yu, H., Yuan, L., Zhou, F., & Tan, Z. (2023). Filtration of dust particles in underground coal mines. *Powder Technology*, *423*, 118506. https://doi.org/10.1016/j.powtec.2023.118506

Jose, J., Patel, J. N., & Patnaik, S. (2015). Application of regression analysis in K-SVD dictionary learning. *Optik*, *126*(20), 2295-2299. https://doi.org/10.1016/j.ijleo.2015.05.133

Kalaiarasan, G., Kumar, P., Tomson, M., Zavala-Reyes, J. C., Porter, A. E., Young, G., ... & Chung, K. F. (2023). Particle Number Size Distribution in Three Different Microenvironments of London. *Atmosphere*, *15*(1), 45. https://doi.org/10.3390/atmos15010045

Kappelt, N., Russell, H. S., Fessa, D., Van Ryswyk, K., Hertel, O., & Johnson, M. S. (2023). Particulate air pollution in the Copenhagen metro part 1: Mass concentrations and ventilation. *Environment International*, *171*, 107621. https://doi.org/10.1016/j.envint.2022.107621

Karwański, M., & Grzybowska, U. (2018). Modeling correlations in operational risk. *Acta Physica Polonica A*, *133*(6), 1402-1407. http://doi.org/10.12693/APhysPolA.133.1402

Khan, M. U., Homan, K. O., Saki, S. A., Emad, M. Z., & Raza, M. A. (2021). Real-time diesel particulate matter monitoring in underground mines: evolution and applications. *International Journal of Mining, Reclamation and Environment*, *35*(4), 291-305. https://doi.org/10.1080/17480930.2020.1818937

Khobragade, R., Singh, S. K., Shukla, P. C., Gupta, T., Al-Fatesh, A. S., Agarwal, A. K., & Labhasetwar, N. K. (2019). Chemical composition of diesel particulate matter and its control. *Catalysis Reviews*. https://doi.org/10.1080/01614940.2019.1617607

Koponen, H., Lukkarinen, K., Leppänen, M., Kilpeläinen, L., Väätäinen, S., Jussheikki, P., ... & Sippula, O. (2023). Applicability of aethalometers for monitoring diesel particulate matter concentrations and exposure in underground mines. *Journal of Aerosol Science*, 106330. https://doi.org/10.1016/j.jaerosci.2023.106330

Kuula, J., Kuuluvainen, H., Niemi, J. V., Saukko, E., Portin, H., Kousa, A., ... & Timonen, H. (2020). Long-term sensor measurements of lung deposited surface area of particulate matter emitted from local vehicular and residential wood combustion sources. *Aerosol Science and Technology*, *54*(2), 190-202. https://doi.org/10.1080/02786826.2019.1668909

Kuuluvainen, H., Rönkkö, T., Järvinen, A., Saari, S., Karjalainen, P., Lähde, T., ... & Keskinen, J. (2016). Lung deposited surface area size distributions of particulate matter in different urban areas. *Atmospheric environment*, *136*, 105-113. https://doi.org/10.1016/j.atmosenv.2016.04.019

Lambrigger, D. D., Shevchenko, P. V., & Wüthrich, M. V. (2009). The quantification of operational risk using internal data, relevant external data and expert opinions. *arXiv preprint arXiv:0904.1361*. https://doi.org/10.48550/arXiv.0904.1361

Lee, K. H., Jung, H. J., Park, D. U., Ryu, S. H., Kim, B., Ha, K. C., ... & Yoon, C. (2015). Occupational exposure to diesel particulate matter in municipal household waste workers. *PLoS one*, *10*(8), e0135229. https://doi.org/10.1371/journal.pone.0135229

Lepistö, T., Kuuluvainen, H., Lintusaari, H., Kuittinen, N., Salo, L., Helin, A., ... & Rönkkö, T. (2022). Connection between lung deposited surface area (LDSA) and black carbon (BC) concentrations in road traffic and harbour environments. *Atmospheric Environment*, *272*, 118931. https://doi.org/10.1016/j.atmosenv.2021.118931

Lepistö, T., Lintusaari, H., Oudin, A., Barreira, L. M., Niemi, J. V., Karjalainen, P., ... & Rönkkö, T. (2023). Particle lung deposited surface area (LDSAal) size distributions in different urban environments and geographical regions: Towards understanding of the PM2. 5 dose–response. *Environment International*, *180*, 108224. https://doi.org/10.1016/j.envint.2023.108224

Leung, C. C., Yu, I. T. S., & Chen, W. (2012). Silicosis. *The Lancet*, *379*(9830), 2008-2018. https://doi.org/10.1016/S0140-6736(12)60235-9

Li, L., Jiang, M., Li, X., & Zhou, B. (2021). Association between Coalmine Dust and Mortality Risk of Lung Cancer: A Meta-Analysis. *BioMed Research International*, *2021*(1), 6624799. https://doi.org/10.1155/2021/6624799

Li, S., Chen, X., Peng, G., Han, M., Guo, Q., Hou, J., & Gao, B. (2023). Research on the Evaluation of Air Quality in Underground Coal Mines Based on a Generalized Contrastive Weighted Comprehensive Scale Index Method. *Atmosphere*, *14*(6), 1021. https://doi.org/10.3390/atmos14061021

Li, Z., Che, W., Lau, A. K., Fung, J. C., Lin, C., & Lu, X. (2019). A feasible experimental framework for field calibration of portable light-scattering aerosol monitors: Case of TSI DustTrak. *Environmental Pollution*, *255*, 113136. https://doi.org/10.1016/j.envpol.2019.113136

Lim, J., Lim, C., & Jung, S. (2021). Characterizations of size-segregated ultrafine particles in diesel exhaust. *Aerosol and Air Quality Research*, *21*(5), 200356. https://doi.org/10.4209/aaqr.200356

Lim, J., Lim, C., & Jung, S. (2021). Characterizations of size-segregated ultrafine particles in diesel exhaust. *Aerosol and Air Quality Research*, *21*(5), 200356. https://doi.org/10.4209/aaqr.200356

Liu, H., Chen, H., Zhang, X., Hu, Y., & Fan, C. (2019). Effects of different factors on the minimum ignition temperature of the mixed dust cloud of coal and oil shale. *Journal of Loss Prevention in the Process Industries*, *62*, 103977. https://doi.org/10.1016/j.jlp.2019.103977

Liu, T., & Liu, S. (2020). The impacts of coal dust on miners' health: A review. *Environmental Research*, *190*, 109849. https://doi.org/10.1016/j.envres.2020.109849

Liu, W., Zhou, Y. (2015). Study of comprehensive evaluation on air quality in mine based on matter element model. *Mineral Resources Development*, *35*, 61–63. (In Chinese)

Liu, X., Hadiatullah, H., Zhang, X., Trechera, P., Savadkoohi, M., Garcia-Marlès, M., ... & Querol, X. (2023). Ambient air particulate total lung deposited surface area (LDSA) levels in urban Europe. *Science of the Total Environment*, *898*, 165466. https://doi.org/10.1016/j.scitotenv.2023.165466

Liu, X., Nie, W., Hua, Y., Liu, C., Guo, L., & Ma, W. (2021). Behavior of diesel particulate matter transport from subsidiary transportation vehicle in mine. *Environmental Pollution*, *270*, 116264. https://doi.org/10.1016/j.envpol.2020.116264

Maleki, S., Sotoudeh, F., & Sereshki, F. (2018). Application of VENTSIM 3D and mathematical programming to optimize underground mine ventilation network: A case study. *Journal of Mining and Environment*, *9*(3), 741-752. https://doi.org/10.22044/jme.2018.6793.1503

McDonald, J. C., Liddell, F. D., Gibbs, G. W., Eyssen, G. E., & McDonald, A. D. (1980). Dust exposure and mortality in chrysotile mining, 1910-75. *Occupational and Environmental Medicine*, *37*(1), 11-24.

Meisel, K., Röver, L., Majer, S., Herklotz, B., & Thrän, D. (2022). A Comparison of functional fillers—greenhouse gas emissions and Air Pollutants from lignin-based filler, carbon black and silica. *Sustainability*, *14*(9), 5393. https://doi.org/10.3390/su14095393

Meng, X., Liu, Y., Wang, J., Wang, Z., & Yan, K. (2022). Experimental study and kinetic analysis on the deflagration characteristics of oil shale dust. *Process Safety and Environmental Protection*, *159*, 830-841. https://doi.org/10.1016/j.psep.2022.01.04

Mesquita, R. F. D., Klein, B., Xavier, A., & Matos, F. R. N. (2017). Mining and the sustainable development goals: a systematic literature review. https://www.researchgate.net/publication/317961722

Monteiro, N. B. R., da Silva, E. A., & Neto, J. M. M. (2019). Sustainable development goals in mining. *Journal of Cleaner Production*, *228*, 509-520. https://doi.org/10.1016/j.jclepro.2019.04.332

Morfeld, P., Lampert, K., Ziegler, H., Stegmaier, C., Dhom, G., & Piekarski, C. (1997). Coal mine dust exposure and cancer mortality in German coal miners. *Applied occupational and environmental hygiene*, *12*(12), 909-914. https://doi.org/10.1080/1047322X.1997.10390627

Noll, J. D., & Birch, E. (2004). Evaluation of the SKC® DPM cassette for monitoring diesel particulate matter in coal mines. *Journal of Environmental Monitoring*, *6*(12), 973-978. https://doi.org/10.1039/b410057c

Panda, S., & Nagendra, S. S. (2018). Chemical and morphological characterization of respirable suspended particulate matter (PM10) and associated heath risk at a critically polluted industrial cluster. *Atmospheric pollution research*, *9*(5), 791-803. https://doi.org/10.1016/j.apr.2018.01.011

Patra, A. K., Gautam, S., & Kumar, P. (2016a). Emissions and human health impact of particulate matter from surface mining operation—A review. *Environmental Technology & Innovation, 5*, 233-249. https://doi.org/10.1016/j.eti.2016.04.002

Patra, A. K., Gautam, S., Majumdar, S., & Kumar, P. (2016b). Prediction of particulate matter concentration profile in an opencast copper mine in India using an artificial neural network model. *Air Quality, Atmosphere & Health, 9*, 697-711. https://doi.org/10.1007/s11869-015-0369-9

Pinssar. *Take control with Pinssar*. 2023 [cited 2023; Available from: https://pinssar.com.au/about/.

Puławska, A., Manecki, M., Flasza, M., & Styszko, K. (2021). Origin, distribution, and perspective health benefits of particulate matter in the air of underground salt mine: a case study from Bochnia, Poland. *Environmental Geochemistry and Health, 43*(9), 3533-3556. https://doi.org/10.1007/s10653-021-00832-2

Ristovski, Z. D., Miljevic, B., Surawski, N. C., Morawska, L., Fong, K. M., Goh, F., & Yang, I. A. (2012). Respiratory health effects of diesel particulate matter. *Respirology*, *17*(2), 201-212. 10.1111/j.1440-1843.2011.02109.x

Roy, D., Singh, G., & Gosai, N. (2015). Identification of possible sources of atmospheric PM 10 using particle size, SEM-EDS and XRD analysis, Jharia Coalfield Dhanbad, India. *Environmental monitoring and assessment, 187*, 1-13. https://doi.org/10.1007/s10661-015-4853-3

Rumchev, K., Hoang, D. V., & Lee, A. (2020). Trends in exposure to diesel particulate matter and prevalence of respiratory symptoms in western australian miners. *International Journal of Environmental Research and Public Health*, *17*(22), 8435. https://doi.org/10.3390/ijerph17228435

Saarikoski, S., Salo, L., Bloss, M., Alanen, J., Teinilä, K., Reyes, F., ... & Timonen, H. (2019). Sources and characteristics of particulate matter at five locations in an underground mine. *Aerosol and Air Quality Research*, *19*(12), 2613-2624. https://doi.org/10.4209/aaqr.2019.03.0118

Saarikoski, S., Teinilä, K., Timonen, H., Aurela, M., Laaksovirta, T., Reyes, F., ... & Hillamo, R. (2018). Particulate matter characteristics, dynamics, and sources in an underground mine. *Aerosol Science and Technology*, *52*(1), 114-122. https://doi.org/10.1080/02786826.2017.1384788

Sabanov, S., Qureshi, A. R., Korshunova, R., & Kurmangazy, G. (2024). Analysis of experimental measurements of particulate matter (PM) and lung deposition surface area (LDSA) in operational faces of an oil shale underground mine. *Atmosphere, 15*(2), 200. https://doi.org/10.3390/atmos15020200

Sabanov, S. (2018). Analysis of field test results for the oil shale mine ventilation simulation. *Oil Shale, 35*(4), 356-364. https://doi.org/10.3176/oil.2018.4.05

Sabanov, S., Magauiya, N., Zeinulla, A., Abil, A., Qureshi, A., Torkmahalleh, M., ... & Rakhimov, D. (2023). Results of diesel exhaust nanoparticle experimental sampling in

a cabin of LHD loader operating in an active ore heading area. In *Underground Ventilation* (pp. 115-119). CRC Press. https://doi.org/10.1201/9781003429241-12

Sabanov, S., Nikitin, O., Qureshi, A., & Dauitbay, Z. (2023b). A case study to improve blasting efficiency by the use of emulsion explosives. *Oil Shale*, (3). https://doi.org/10.3176/oil.2023.3.05

Sabanov, S., Qureshi, A. R., Dauitbay, Z., & Kurmangazy, G. (2023a). A Method for the Modified Estimation of Oil Shale Mineable Reserves for Shale Oil Projects: A Case Study. *Energies*, *16*(16), 5853. https://doi.org/10.3390/en16165853

Salo, L. (2023). Characterization and Development of Electrical Methods for Aerosol Measurement. http://urn.fi/URN:ISBN:978-952-03-2930-3

Salo, L., Rönkkö, T., Saarikoski, S., Teinilä, K., Kuula, J., Alanen, J., ... & Keskinen, J. (2021). Concentrations and size distributions of particle lung-deposited surface area (LDSA) in an underground mine. *Aerosol and Air Quality Research*, *21*(8), 200660. https://doi.org/10.4209/aaqr.200660

Sarver, E., Keles, C., & Rezaee, M. (2019). Beyond conventional metrics: Comprehensive characterization of respirable coal mine dust. *International Journal of Coal Geology*, *207*, 84-95. https://doi.org/10.1016/j.coal.2019.03.015

Schauer, J. J. (2003). Evaluation of elemental carbon as a marker for diesel particulate matter. *Journal of Exposure Science & Environmental Epidemiology*, *13*(6), 443-453. https://doi.org/10.1038/sj.jea.7500298

Schiavo, B., Morton-Bermea, O., Meza-Figueroa, D., Acosta-Elías, M., González-Grijalva, B., Armienta-Hernández, M. A., ... & Valera-Fernández, D. (2023). Characterization and Polydispersity of Volcanic Ash Nanoparticles in Synthetic Lung Fluid. *Toxics*, *11*(7), 624. https://doi.org/10.3390/toxics11070624

Schmid, O., & Stoeger, T. (2016). Surface area is the biologically most effective dose metric for acute nanoparticle toxicity in the lung. *Journal of Aerosol Science*, *99*, 133-143. https://doi.org/10.1016/j.jaerosci.2015.12.006.

Schriefl, M. A., Nishida, R. T., Knoll, M., Boies, A. M., & Bergmann, A. (2020). Characterization of particle number counters based on pulsed-mode diffusion charging. *Aerosol Science and Technology*, *54*(7), 772-789. https://doi.org/10.1080/02786826.2020.1724257

Shi, L.; Yu, X.; Mi, T.; Wu, X.; Yang, H. (2006). Assessment on mine air quality using pollution loss rate. *Industrial Safety and Environmental Protection*, *32*, 36–37. (In Chinese)

Shrestha, G., Traina, S.J., Swanston, C.W., 2010. Black carbon's properties and role in the environment: a comprehensive review. Sustainability 2, 294-320. https://doi.org/10.3390/su2010294

Silvester, S. A., Lowndes, I. S., & Hargreaves, D. M. (2009). A computational study of particulate emissions from an open pit quarry under neutral atmospheric conditions. *Atmospheric Environment*, *43*(40), 6415-6424. https://doi.org/10.1016/j.atmosenv.2009.07.006

Straif, K., Benbrahim-Tallaa, L., Baan, R., Grosse, Y., Secretan, B., El Ghissassi, F., ... & Cogliano, V. (2009). A review of human carcinogens—part C: metals, arsenic, dusts, and fibres. *The lancet oncology*, *10*(5), 453-454. https://doi.org/ 10.1016/S1470-2045(09)70134-2

Timonen, H., Teinilä, K., Aurela, M., Reyes, F., Vásquez, Y., Bloss, M., ... & Saarikoski, S. (2018). Sources and composition of particulate matter in boreal arctic environment next to an active mining area. *Boreal Environment Research*, *23*(1-6), 105.

Todea, A. M., Beckmann, S., Kaminski, H., & Asbach, C. (2015). Accuracy of electrical aerosol sensors measuring lung deposited surface area concentrations. *Journal of Aerosol Science*, *89*, 96-109. https://doi.org/10.1016/j.jaerosci.2015.07.003

Tran, P. T. M., Ngoh, J. R., & Balasubramanian, R. (2020). Assessment of the integrated personal exposure to particulate emissions in urban micro-environments: A pilot study. *Aerosol and Air Quality Research*, *20*(2), 341-357. https://doi.org/10.4209/aaqr.2019.04.0201

Trechera, P., Moreno, T., Córdoba, P., Moreno, N., Zhuang, X., Li, B., ... & Querol, X. (2020). Mineralogy, geochemistry and toxicity of size-segregated respirable deposited dust in underground coal mines. *Journal of Hazardous Materials*, *399*, 122935. https://doi.org/10.1016/j.jhazmat.2020.122935

Turner, S. (2007). Diesel particulate exposure and control in western australia underground mines

van Zijverden, M., van der Pijl, A., Bol, M., van Pinxteren, F. A., de Haar, C., Penninks, A. H., ... & Pieters, R. (2000). Diesel exhaust, carbon black, and silica particles display distinct Th1/Th2 modulating activity. *Toxicology and Applied Pharmacology*, *168*(2), 131-139. https://doi.org/10.1006/taap.2000.9013

Ventsim Design User Guide [Online PDF]

Volkwein, J., Hansen, A. D. A., & Hill, J. (2016). New sensor for continuous tracking of diesel particulate matter in mines to optimize mine ventilation system.

Volkwein, J., Robertson, K., & Hansen, A. D. A. (2017). Long-term continuous measurement of diesel particulate matter patterns in a large underground metal mine. In *Proceedings 16th North American Mine Ventilation Symposium* (pp. 5-19).

Vouitsis, E., Ntziachristos, L., & Samaras, Z. (2003). Particulate matter mass measurements for low emitting diesel powered vehicles: what's next?. *Progress in Energy and Combustion Science*, *29*(6), 635-672. https://doi.org/10.1016/j.pecs.2003.08.002

Wang, J., Meng, X., Ma, X., Xiao, Q., Liu, B., & Zhang, G. (2019a). Experimental study on whether and how particle size affects the flame propagation and explosibility of oil shale dust. *Process Safety Progress*, *38*(3), e12075. https://doi.org/10.1002/prs.12075

Wang, Z., Li, S., Ren, T., Wu, J., Lin, H., & Shuang, H. (2019b). Respirable dust pollution characteristics within an underground heading face driven with continuous miner–A CFD modelling approach. *Journal of Cleaner Production*, *217*, 267-283. https://doi.org/10.1016/j.jclepro.2019.01.273

Widodo, N. P., Putra, S. H., Ihsan, A., Gautama, R. S., Cheng, J., Waly, F. Z., & Permadi, D. A. (2023). The study of coal dust minimum explosion concentration of subbituminous coal. *Process Safety and Environmental Protection*, *177*, 1387-1392. https://doi.org/10.1016/j.psep.2023.08.002

World energy outlook 2022. (2022). *World Energy Outlook*. https://doi.org/10.1787/3a469970-en

Xu, G., Chang, P., Mullins, B., Zhou, F., & Hu, S. (2018). Numerical study of diesel particulate matter distribution in an underground mine isolated zone. *Powder technology*, *339*, 947-957. https://doi.org/10.1016/j.powtec.2018.08.075

Ye, Y., Ding, D., Li, X., & Zhou, X. (2007). An evaluation model for air quality in underground uranium mines based on integrated scale index on weights of generalized contrast. *Uranium Mining and Metallurgy*, *26*(4), 197-200. http://inis.iaea.org/search/search.aspx?orig_q=RN:41073500

Yu, L., Li, G., Liu, W., Yu, J., & Yuan, C. (2017). Experimental investigations on ignition sensitivity of hybrid mixtures of oil shale dust and syngas. *Fuel*, *210*, 1-7. https://doi.org/10.1016/j.fuel.2017.06.082

Zhang, L., Zhou, G., Ma, Y., Jing, B., Sun, B., Han, F., ... & Chen, X. (2021). Numerical analysis on spatial distribution for concentration and particle size of particulate pollutants in dust environment at fully mechanized coal mining face. *Powder Technology*, *383*, 143-158. https://doi.org/10.1016/j.powtec.2021.01.039